PHILOSOPHICAL TRANSACTIONS OF THE ROYAL SOCIETY A MATHEMATICAL, PHYSICAL & ENGINEERING SCIENCES

The Breakdown of Superfluidity in Liquid ^{4}He V. Measurement of the Landau Critical Velocity for Roton Creation

T. Ellis and P. V. E. McClintock

Phil. Trans. R. Soc. Lond. A 1985 **315**, 259-300
doi: 10.1098/rsta.1985.0041

Phil. Trans. R. Soc. Lond. A **315**, 259–300 (1985) [259]
Printed in Great Britain

THE BREAKDOWN OF SUPERFLUIDITY IN LIQUID ^{4}He V*. MEASUREMENT OF THE LANDAU CRITICAL VELOCITY FOR ROTON CREATION

By T. Ellis and P. V. E. McClintock
Department of Physics, University of Lancaster, Lancaster LA1 4BY, U.K.

(*Communicated by W. F. Vinen, F.R.S.* – *Received* 22 *October* 1984)

CONTENTS

* Parts I–IV appeared respectively in *Phil. Trans. R. Soc. Lond.* A **284**, 179–224 (1977); *Phil. Trans. R. Soc. Lond.* A **296**, 581–595 (1980); *Phil. Trans. R. Soc. Lond.* A **307**, 201–260 (1982) and *Phil. Trans. R. Soc. Lond.* A **313**, 537–606 (1985).

We report a precise experimental determination of the Landau critical velocity v_L for roton creation in HeII. The technique used was based on measurements of the drift velocity, $\bar{v}$, of negative ions through isotopically pure liquid ^{4}He at *ca.* 80 m K, under the influence of weak electric fields, E, for pressures, P, within the range $13 \leqslant P \leqslant 25$ bar. It relied on the use of the equation $(\bar{v}-v_L) \propto E^{\frac{1}{3}}$, which is believed to correspond to the creation of rotons occurring predominantly in pairs and which fitted the experimental data to very high precision for $E > 500$ V m^{-1}. At lower values of E, however, small deviations from this equation were observed. These are tentatively attributed, not to the predicted onset of single-roton emission, but to a novel form of ion-vortex scattering. The values of $v_L(P)$ deduced from the measurements of $\bar{v}(E)$ at various pressures for $E > 500$ V m^{-1} agree to within 1.5% with theoretical predictions based on Landau's excitation model of HeII, incorporating accepted numerical values of the roton parameters. The observed pressure dependence of $v_L(P)$ is significantly stronger than that predicted; however, a discrepancy that appears to point towards the decreasing accuracy with which the roton parameters are known at high pressures. The modulus of the matrix element $|V_{k_0, k_0}|$ characterizing roton-pair emission has also been deduced and is found to decrease rapidly with falling pressure. A linear extrapolation of the data suggests that $|V_{k_0, k_0}|$ falls to zero at $P \approx 3$ bar (1 bar $= 10^5$ Pa).

1. Introduction

(a) *Background, aims and objectives*

The Landau critical velocity, v_L, represents the minimum velocity at which a massive moving object can dissipate its kinetic energy by creating excitations in the medium through which it is travelling. The existence of a finite value for v_L in liquid ^{4}He is therefore an essential prerequisite for its superfluidity. As discussed in detail in the first paper in this series (Allum *et al.* 1977; hereinafter referred to as I), it is possible to relate v_L to the dispersion curve for the elementary excitations. Thus a precise experimental determination of v_L can yield information about the dispersion curve complementary to that acquired through inelastic neutron scattering, or from measurements of thermal properties. Alternatively a comparison of the measured and predicted values of v_L can be regarded as a particularly direct and illuminating test of Landau's excitation model of HeII.

Although the Landau critical velocity is clearly one of the fundamental parameters of liquid ^{4}He, no satisfactory experimental determination of this quantity has hitherto been achieved. Several experiments have, however, demonstrated that it does exist and takes approximately the predicted value (I and references to earlier work therein; Andrei & Glaberson 1980 (close to the lambda transition where v_L becomes very small)). There are a number of technical reasons why the measurement of v_L has proved to be an unexpectedly difficult one, and we will refer to some of these in detail below. Fortunately it has recently proved possible to circumvent most of the problems in question and the main purpose of the present paper is to report that we have succeeded in making precise measurements of v_L over a wide range of pressures, and to discuss these in the context of existing theories of HeII.

As already discussed in I, negative ions apparently constitute the only type of probe for which the drift velocity $\bar{v}$ can be raised beyond v_L without the occurrence of an extremely rapid transition to quantized vortex rings. It was found that measurements of $\bar{v}$ for the normal negative ion were consistent with

$$\bar{v} = v_L + AE^{\frac{1}{3}}, \tag{1.1}$$

where E is the applied electric field and A is a constant that depends on pressure, an observation that was taken to indicate that the ions create rotons *in pairs* when $\bar{v} \geqslant v_L$. This inference received additional support when the measurements of $\bar{v}(E)$ were subsequently extended to extremely high electric fields (Ellis *et al.* 1980*a*; hereinafter referred to as II). The large deviations that were then observed from (1.1) were found to be in excellent agreement with predictions based on the roton-pair emission theory of Bowley & Sheard (1977) (hereinafter referred to as the BS theory).

That rotons should apparently be created only in pairs by a moving ion came as a complete surprise and still awaits a physical explanation. It may be surmized, however, that this unexpected selection rule relates to some fundamental, but as yet unappreciated, property of the roton itself. If single-roton emission can in fact occur, albeit as a weakly allowed process, evidence for its existence is most likely to be found in measurements of $\bar{v}(E)$ made in extremely weak electric fields and a search for such evidence formed an important additional motivation for the work described below.

The third and fourth papers in this series on the breakdown of superfluidity in ^{4}He are by Bowley *et al.* (1982; hereinafter referred to as III), on the nucleation of quantum vortices by negative ions in isotopically pure ^{4}He and by Nancolas *et al.* (1985, hereinafter referred to as IV) on the influence of ^{3}He isotopic impurities on the vortex nucleation process. As we shall see, these papers are of direct relevance to the present work. This is because the success of attempts to measure $\bar{v}(E)$ in weak electric fields at low temperatures turns out to be crucially dependent on every possible effort being made to maximize the ratio of bare ions to charged vortex rings within the experimental cell.

In §1*b* of this paper we extend the treatment of I so as to discuss in a more detailed way how v_L relates to the shape of the dispersion curve and, in §1*c*, we describe briefly the interesting phenomena that are to be anticipated if roton-pair emission gives way to single-roton emission in sufficiently weak electric fields. In §2*a* we discuss the general physical considerations governing the design of the experiments and in §§2*b*–*d* we outline how these have influenced the structure of the experimental cell, the electrical circuitry and the cryogenic and gas handling arrangements used in practice. Measurements of $\bar{v}$ have in fact been made in a number of different ways to optimize their precision under varying conditions of electric field and pressure. In §2*e*, we describe the basis of the technique used for all the velocity measurements and in §2*f* we discuss how it was applied to the particular case of the absolute determination of the velocity. The latter variant of the technique worked to best effect in moderate or relatively strong electric fields. At lower electric fields, where the magnitudes of the signals became much smaller, we have found it highly advantageous to use a cross-correlation technique that measures very precisely, not the absolute value of the velocity, but the change in velocity relative to a reference signal recorded in a stronger field: we describe this technique in §2*g*. An enduring difficulty associated with the study of ions in liquid helium in very weak fields has stemmed (Schwarz 1972) from what appears to be a reduced 'transparency' of the control grids, manifesting itself as a severe attenuation of the ion signal. In §2*h* we discuss the basis of a transient low-field method that we have developed to evade this particular problem.

The experimental results are presented in §3. In §3*a* we show examples of ion signals acquired under a range of different conditions and in §3*b* we present the velocity measurements that can be deduced from those above and below a field of *ca.* 500 V m^{-1}. We shall see that the

behaviour of $\bar{v}(E)$ is quite different in these two ranges. A brief discussion of the experimental uncertainties is given in §3*c*.

A discussion and analysis of the $\bar{v}(E)$ data is presented in §4. We will see in §§4*a*, *b* that, subject to certain underlying assumptions, precise values of v_L and of the matrix element for roton-pair emission may be deduced from the data for $E > 500$ V m^{-1}, over a wide range of pressures. Velocity data at lower fields, which exhibit a rather different field dependence, are discussed in §4*c*. Finally, in §5, we try to sum up succinctly what has been learned and to point out some important matters that still remain to be elucidated. Some selected numerical data are presented in tabular form in the Appendix.

(*b*) *The dispersion curve and the Landau critical velocity*

Landau showed that a massive object travelling through HeII at an initial velocity v can create an excitation of energy ϵ and momentum $\hbar k$ while conserving the total energy and local momentum, if and only if $v > \epsilon/\hbar k$, so that there is a critical velocity v_L for the process given by

$$v_L = (\epsilon/\hbar k)_{\min}. \tag{1.2}$$

Landau's arguments, and their implications, were discussed in detail in I and need not be repeated here. It was shown that the value of v_L is given by the gradient of a straight line drawn from the origin to make a tangent with the dispersion curve near the roton minimum and that it is given, to a good approximation, by the ratio $\Delta/\hbar k_0$, where Δ and $\hbar k_0$ are respectively the energy and momentum of a roton at the minimum. The accuracy of the measurements to be described below is such, however, that this approximation is no longer sufficient. To find a more accurate expression for v_L, we seek the condition that the straight line

$$\epsilon = v\hbar k \tag{1.3}$$

makes a tangent with the roton region of the dispersion curve, which we can approximate by the parabola

$$\epsilon = \Delta + \hbar^2(k-k_0)^2/(2\mu), \tag{1.4}$$

where μ is the effective mass of a roton. It is straightforward to demonstrate that this condition will be fulfilled for $v = v_L$ where

$$v_L = [(2\Delta\mu + \hbar^2 k_0^2)^{\frac{1}{2}} - \hbar k_0]/\mu. \tag{1.5}$$

This is the required expression, with which we will compare our experimental measurements of v_L in §4. Insertion into (1.5) of accepted values of the Landau roton parameters shows immediately that v_L changes to a considerable extent with the pressure applied to the liquid. The solid curve of figure 1, based on the set of parameters compiled by Brooks & Donnelly (1977), shows that v_L varies from *ca.* 60 m s^{-1} at the saturated vapour pressure to *ca.* 45 m s^{-1} just below the solidification pressure. As we shall see, the roton parameters are very precisely determined at the saturated vapour pressure; but there exists significant uncertainty as to the best values to assume at elevated pressures, with corresponding uncertainties in the theoretical value of v_L.

Finally, in this section, it should be recalled (see I) that the minimum velocity at which an object of mass m can create a roton actually exceeds v_L, as defined by (1.2) and hence by (1.5), by an increment *ca.* $\hbar k_0/2m$. For a massive object this increment is, of course, negligible; but for relatively light objects, such as ions, it is extremely important and must be taken fully into account. The velocity decrement suffered by the object ($\hbar k_0/m$) during roton emission is such,

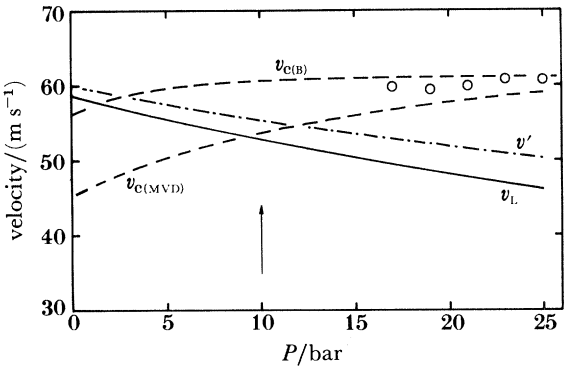

FIGURE 1. Critical velocities in HeII plotted as a function of pressure, P. The solid curve represents the predicted Landau critical velocity, V_L, and the chained curve shows the corresponding critical velocity v' above which the normal negative ion is energetically able to create a pair of rotons (see I). The two broken curves represent the calculations of Muirhead *et al.* (1984) and Bowley (1984) of the critical velocity v_c above which the normal negative ion is energetically able to nucleate vortex rings in HeII, indicated respectively by the subscript MVD and B in parentheses. The circled points are measured values of v_c taken from III. Earlier experiments (see text) suggest that, in reality, the $v'(P)$ and $v_c(P)$ curves ought to cross over at *ca.* 10 bar, as indicated by the vertical arrow. (1 bar = 10^5 Pa.)

however, that its threshold drift velocity for roton creation is nonetheless closely equal to v_L. In the case of roton-pair emission, which we believe to be overwhelmingly more probable than single-roton emission under normal circumstances, the threshold instantaneous velocity is $v_L + \hbar k_0/m$ and the recoil velocity decrement is $2\hbar k_0/m$ so that again the threshold drift velocity is closely equal to v_L.

(*c*) *Single-roton emission*

The basis of the technique used for the determination of v_L lies in fitting precise measurements of $\bar{v}(E)$ to (1.1), so that the intercept then yields v_L directly. The method is, in principle, entirely straightforward; but it must be admitted that it relies upon assumptions for which no justification exists *a priori* and on an argument that is, to a certain extent, a circular one. In particular, our intended use of (1.1) rests on the assumption that momentum loss from the moving ion occurs exclusively, or at least predominantly, through roton-pair emission. Yet the pair emission inference itself arose directly from the observation that the early experimental data, which were considerably less accurate than those to be reported below, could be described within experimental error by an equation of the form of (1.1). The circular nature of this argument is lessened, however, by the fact that, as already mentioned above, values of $\bar{v}(E)$ measured in very strong fields depart to a marked extent from those predicted by (1.1) but are still extremely well described by a (slightly extended) form of the BS theory (see II). To this extent, we can regard the pair-emission hypothesis as having received additional support through independent measurements.

Some further reservations and comments about the use of (1.1) for the measurement of v_L should also be entered. First, we must point out that Iordanskii (1968) derived an equation of the same form as (1.1) on the assumption of single-roton emission. We believe, however, that the premises upon which his theory is based do not correspond to the real physical situation as revealed subsequently by the experiments of I. In particular, the theory is, of its essence, based on a strong coupling model in which the drag due to roton emission would increase

extremely rapidly above the threshold velocity, an assumption that is clearly at variance with our experimental observation that $\bar{v}$ exceeds v_L by several metres per second even in relatively modest electric fields. These considerations are not, however, of direct relevance to the measurement of v_L itself: provided only that the relation (1.1) is followed, regardless of the details of the physical mechanism that may be involved, we may still use the equation to extract a value of v_L from a set of precise measurements of $\bar{v}(E)$.

Secondly, even if we accept that rotons are created predominantly in pairs within the range of electric fields covered by the experiments of I, there remains the possibility that single-roton emission might still become important in weaker electric fields and consequently give rise to deviations from (1.1). In weaker fields the average time interval during which the velocity of the accelerating ion of mass m_i exceeds the threshold velocity

$$v_1' = v_L + \hbar k_0/2m_i \tag{1.6}$$

for single-roton emission, but remains below the threshold

$$v_2' = v_L + \hbar k_0/m_i \tag{1.7}$$

for roton-pair emission will, of course, be larger and it is under these conditions, if at all, that single-roton emission is most likely to manifest itself. Thus, if each of the two emission processes is allowed to occur in principle, but the matrix element characterizing single-roton emission is very small compared with that for pair emission, then there is bound to be a characteristic electric field at which the dominance of one process gives way to that of the other. The resultant deviations from (1.1), which may be expected to be quite complicated, are of considerable intrinsic interest in their own right and have been discussed in detail by Sheard & Bowley (1978). Here we will just summarize the main features that are of relevance to the present experiment.

In figures 2*a* and *b* we sketch the instantaneous velocity of the ion as a function of time close to the critical field where, within the approximation of an average pre-emission time (see I), single-roton emission gives way to roton-pair emission. In figure 2*a*, the ion emits a single roton just before it reaches the pair-emission threshold velocity v_2' (suffering a velocity decrement of $\hbar k_0/m$ in the process) and then accelerates again: its drift velocity will be slightly less than v_1'. In figure 2*b*, after a marginal increase in the electric field, the whole trajectory has risen slightly so that, on average, the ionic velocity has exceeded v_2' before the ion has emitted a roton. Because the roton-pair emission process is so strongly favoured over single-roton emission, the ion emits a pair of rotons almost immediately after attaining v_2' and consequently suffers a velocity decrement twice as large as that in *a*; its drift velocity will thus have decreased and will be only marginally in excess of v_L. If, therefore, we plot the expected drift velocity as a function of $E^{\frac{2}{3}}$ over a range of weak electric fields, we might expect to see the type of behaviour depicted in figure 2*c*. To begin with, $v(E^{\frac{2}{3}})$ follows a straight line in accordance with the equation (see I)

$$\bar{v} = v_L + BE^{\frac{2}{3}}. \tag{1.8}$$

At the onset field for pair emission, however, there will be a sudden discontinuous decrease in $\bar{v}$ as illustrated.

In reality, of course, there will always be a certain spread in the instantaneous ionic velocities at which roton emission occurs, so that the concept of an average pre-emission time actually represents something of an over-simplification. A more accurate description of the phenomenon

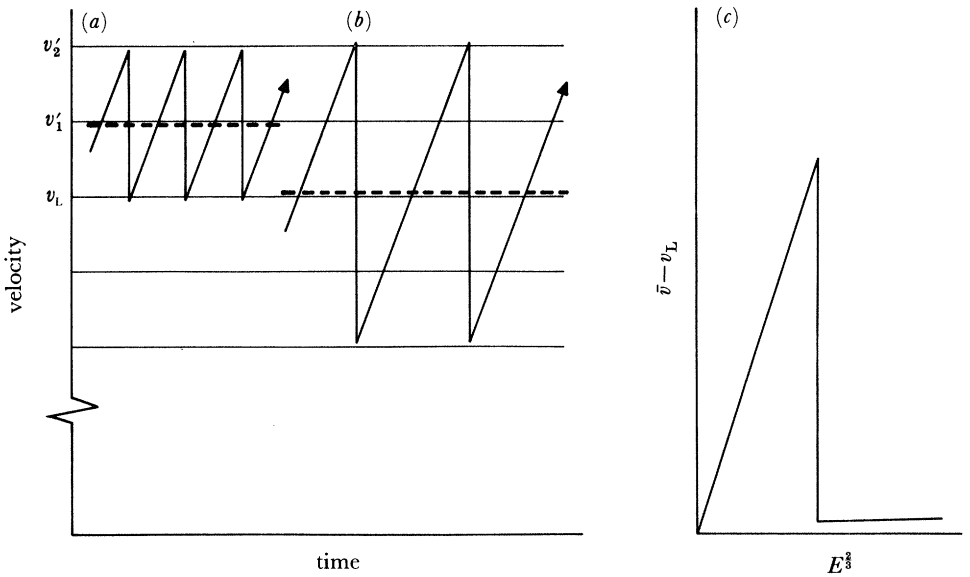

FIGURE 2. A simple explanation of the effect on the ionic drift velocity of the transition from single-roton to roton-pair emission. The ionic drift velocity (indicated by the heavy broken lines) decreases at the transition as sketched in (*c*). A detailed calculation, based on the use of a Boltzmann equation, implies a region of negative resistance (figure 3) rather than the discontinuous drop in velocity suggested by this simple model.

requires a solution of the appropriate Boltzmann transport equation and this leads, not unexpectedly, to a somewhat less dramatic manifestation of negative resistance than that sketched in figure 2*c*. The result of Sheard & Bowley's detailed calculation is shown in figure 3. The several different curves correspond, not to different ratios of the single- and pair-emission matrix elements (which have different dimensions and therefore cannot be compared directly), but to different ratios of the rate constant K_1 and K_2. These are defined in terms of the transition rates R_1 and R_2 for the two processes as

$$R_1(v) = K_1[(v-v_1')/v_L]^{\frac{1}{2}} \tag{1.9}$$

and

$$R_2(v) = K_2[(v-v_2')/v_L]^2 \tag{1.10}$$

and their relations to the matrix elements are given by equations (18), (19), (43) and (44) of I. Although the predicted behaviour is rather less striking than that implied by figure 2*c*, there is still a region of negative resistance for small enough values of K_1/K_2.

Also shown in figure 3 are some of the experimental velocity data of I. These are subject to considerable scatter, mainly because of the relative shortness (10 mm) of the experimental cell then in use; more seriously, they 'droop' at low electric fields because of the combined effects of the scattering of thermal excitations and of ^{3}He quasiparticles in HeII of the natural isotopic ratio at 0.35 K. The latter effects would clearly have precluded detection of any of the interesting phenomena predicted by Sheard & Bowley to occur in the region where single-roton emission gives way to pair emission. The present work, however, has been performed under conditions such that the effects of ^{3}He and excitation scattering should have been negligible. It was hoped, therefore, that if deviations were found to occur from (1.1) in very weak electric fields, it would prove possible to interpret these in terms of the onset of the elusive single-roton emission process.

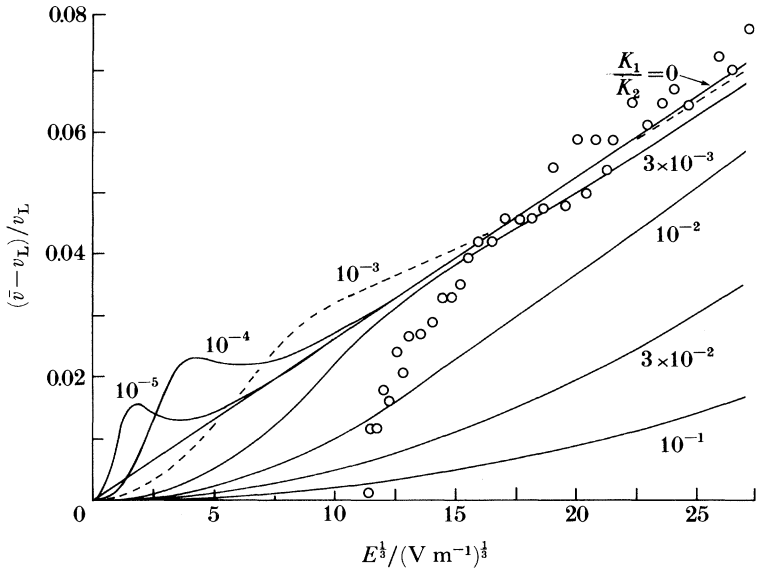

FIGURE 3. Deviations from (1.1) resulting from the onset of single-roton emission at very low electric fields, after Sheard & Bowley (1978). The calculated fractional difference between the ionic drift velocity $\bar{v}$ and the Landau critical velocity v_L is plotted as a function of $E^{\frac{1}{3}}$ for several different ratios of the single-roton and roton-pair emission rates K_1 and K_2, respectively, as indicated by the number adjacent to each curve. The circled points represent velocity data from the experiments of I, which were clearly too imprecise and at too high a temperature to have detected the predicted deviations.

2. EXPERIMENTAL DETAILS

(*a*) *General design considerations*

The experimental technique used for determination of the ionic drift velocity, derived from the single-pulse method introduced by Schwarz (1972), was similar to that already described in connection with the measurements of I and II. Ions were injected into the sample of HeII by field emission; their initial entry into a region of uniform electric field (the 'drift space') could be controlled by means of a transient change in the potential difference between a pair of gate grids; and, as they finally passed through a screening grid at the other end of the drift space, they induced a signal in the closely adjacent collecting electrode. From a measurement of the ionic transit time, and a knowledge of the length of the drift space, the average velocity, $\bar{v}$, of the ions could immediately be found.

There were also, however, a number of important differences from the experimental arrangements of I and II. First, to facilitate velocity measurements of improved absolute accuracy, we have designed a cell in which the length, L, of the drift space is much more precisely determined than were those in I and II (where uncertainties in L constituted by far the largest source of systematic error in the measured values of $\bar{v}$). Secondly, we have made provision for extension of the velocity measurements down to very much weaker electric fields than were possible in I, partly to reduce the range over which $\bar{v}(E)$ must be extrapolated in the determination of v_L from (1.1) and partly, as discussed above, to enable a search to be made for possible evidence of the occurrence of single-roton emission processes. It is the requirement for measurements in extremely weak electric fields that has particularly influenced many vital features of the overall experimental design.

It is immediately evident from the small sample of data from I (figure 3), that a reduction in the temperature of the sample was an essential prerequisite for measurements of the roton-emission-limited drift velocity in weaker electric fields, to reduce the drag caused by excitation scattering. The maximum permissible temperature for measurements of given accuracy at any particular electric field is not easy to estimate *a priori* (and it should be noted that the drag coefficients measured at higher temperatures in III referred to roton scattering, not to the phonon scattering that is dominant in the temperature range of the present work). We may, however, take as a very approximate rule of thumb the requirement that the temperature be such that $\mu(T) \gg v_L/E$, where $\mu(T)$ is the zero-field mobility. Precise values of μ have been determined for negative ions over a range of pressures (Ostermeier 1973), but only down to 0.28 K where they were, in any case, already becoming too large to measure without difficulty. Unfortunately, it is far from straightforward to extrapolate these data reliably to lower temperatures, partly because, as discussed in detail by Ostermeier, ion–phonon scattering is characterized by a complicated frequency dependence. Instead, we have simply plotted, on a double logarithmic scale in figure 4, Ostermeier's four lowest temperature measurements of μ (data at higher temperatures being significantly influenced by roton scattering) at two pressures, together with our guesses as to how $\mu(T)$ might behave at lower temperatures. We conclude from such plots that, for reliable measurements of the roton-emission-limited $\bar{v}(E)$ at $E = 50$ V m^{-1}, we would probably need to ensure that $T < 110$ and $T < 130$ m K at $P = 13$ and 25 bar, respectively. It must be emphasized that there is no physical basis for the extrapolations of figure 4. They serve as a useful semi-quantitative guide to the sort of behaviour that might reasonably be anticipated and, as such, they are of value

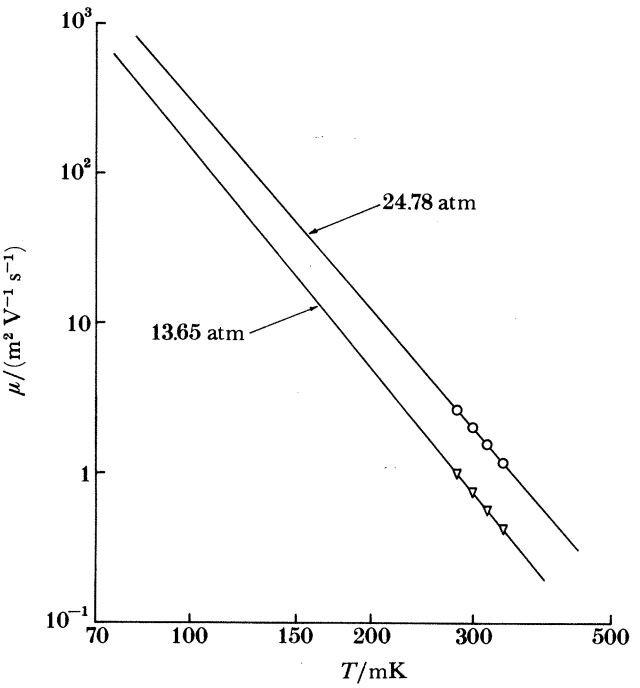

FIGURE 4. Extrapolation of Ostermeier's (1973) mobility measurements to lower temperatures to estimate the maximum temperature at which Landau velocity measurements can reliably be made. The ionic mobility, μ, of the negative ion is plotted for two pressures as a function of the temperature T. It should be noted that both axes have logarithmic scales.

in the design of the experiment. In the last resort, however, it is clearly essential to determine by direct measurement the range of physical conditions within which $\bar{v}(E)$ can be considered to remain temperature-independent: such measurements are presented below in §3*a* and, as we shall see, they turn out to be not inconsistent with our expectations based on figure 4.

In common with the earlier sections of the research programme, it is to be expected that the pressure range over which $v_L(P)$ can be followed will be limited at its lower end by the rapid conversion of bare ions to charged vortex rings (and the upper limit will, of course, be set by solidification of the helium, just above 25 bar). The reason for the apparent impossibility of propagating bare ions in HeII at low pressures and millikelvin temperatures seems to be related to the opposed pressure dependence of v_L and of the critical velocity v_c for creation of a vortex ring (see III). It appears that, as indicated in figure 1, the curves for $v_c(P)$ and $v_L(P)$ cross at a pressure somewhere in the vicinity of 10 bar. Strictly, the relevant roton-creation velocity is not v_L itself (which, as discussed above, refers to an object of infinite mass) but, rather, is $v' = v_L + \hbar k_0/m_i$, the critical velocity that the ion of mass m_i must attain to create a roton, represented in figure 1. The increase in the separation of $v'(P)$ from $v_L(P)$ with increasing pressure occurs because of the decrease in the radius of the ion, which in turn gives rise to a corresponding decrease in its hydrodynamic effective mass m_i (Ellis *et al.* 1983).

For pressures such that $v' < v_c$, it is possible for an ion to travel over relatively large distances without creating a vortex ring. In a weak electric field its velocity, limited by roton emission, will not on average attain the value of v_c required for ring nucleation (although it may be expected that the ion will create a ring eventually, as a result of the high velocity tail on the distribution function (Bowley & Sheard 1977)). When $v' > v_c$, on the other hand, the accelerating ion exceeds the critical velocity for ring nucleation before it attains the roton-creation velocity. It is therefore likely to undergo the transition to a charged vortex ring very rapidly indeed, even in extremely weak electric fields. A distinct change in the behaviour of the ion is therefore to be anticipated at the pressure where $v'(P)$ crosses $v_c(P)$.

Unfortunately, the pressure dependence of $v_c(P)$ is not accurately known. The high-pressure experimental values that were deduced in III are shown as the circled points in figure 1 and the calculations of $v_c(P)$ by Muirhead *et al.* (1984) and by Bowley (1984) are indicated by the lower and upper broken curves respectively. It would thus appear that the cut-off pressure for bare ions lies somewhere between 12 and 3 bar. In practice, the experiments of III could not be extended below 15 bar, but this limitation is believed to have been a result of vortex nucleation close to the field-emission tips, where the electric field is always very high during the relevant period of the emission cycle. The early experiments of Rayfield (1966) suggest that the cut-off actually lies between 10 and 12 bar; measurement of the pressure dependence of the field-emission current (Phillips & McClintock 1973) imply a value of 10 or 11 bar. On this basis, we may guess that Bowley's calculated $v_c(P)$ curve lies too high (there being, in fact, considerable uncertainty as to its absolute magnitude) and that the curve of Muirhead *et al.* is slightly too low (which would also be consistent with its relation to the data points at high pressure). In this work, therefore, we may hope at least to be able to follow the pressure dependence of v_L down to a pressure somewhat above 10 bar, but there is clearly not much chance of any extension of the measurements to pressures lower than this.

In the light of the vortex-nucleation rate measurements that were reported in IV, it can quickly be shown to be essential for the sample of ^{4}He to be isotopically purified. For example, figure 4*d* of IV shows that, in the case of helium of approximately the natural isotopic ratio

and for an electric field of 10^4 V m^{-1}, the nucleation rate ν has reached 8×10^3 s^{-1} at 0.33 K and is rising rapidly with decreasing temperature. For the present experiments, with a drift space of length 0.1 m, a value of $\nu \approx 10^3$ s^{-1} (which would result in the loss of *ca.* 90 % of the bare ions) is probably about the highest nucleation rate that is tolerable. The only way to ensure that ν will be smaller than this at 100 m K is to remove the ^{3}He, an action that, as discussed in III, results in a value of ν that is both considerably reduced and also apparently temperature-independent below *ca.* 0.5 K. The extreme sensitivity of ν to the ^{3}He:^{4}He ratio, x_3, means that a very high standard of isotopic purity is needed. We estimate that, to be reasonably certain of success, it is necessary to ensure that x_3 is less than about 10^{-10}, at which concentrations the ionic mean free path for interactions with the ^{3}He will have become greater than the length of the drift space.

Because of the relatively low electric fields in which measurements are needed, particular care is required to avoid problems arising from the building up of charge on dielectrics within the cell, either on the nylon insulators that separate the electrodes or on insulating layers of oxide or dirt on the surfaces of the electrodes themselves. The first of these considerations can be accommodated by very careful design of the cell geometry (see §2*b*) and the second by the gold plating and scrupulous cleaning of all electrodes.

It is clearly essential to ensure that the density of ions in the drift space should always be such that space–charge effects can be ignored; that is, the net force on any given ion arising from the electrostatic repulsion of all the other ions in the propagating ion cloud should always be much less than that from the applied electric field. In practice, the criterion clearly becomes progressively harder to meet as the measurements are extended to lower electric fields, because the necessarily reduced ion densities will give rise to weaker signals and consequently to the need for correspondingly longer averaging periods to achieve any given ratio of signal:noise. To get some idea of the maximum signal current that can be used safely for any given applied field, we have calculated the magnitude of the space–charge field at the edge of the charge disk where it takes its largest value. In doing so, we have assumed that the density of charge within the disk is radially homogenous but that it exhibits an approximately gaussian variation along the direction of propagation. The result is shown by the solid line of figure 5. Also shown in the figure are some typical values of applied electric field and signal current used in practice: the applied electric field was always larger by a factor of at least 100 than the space–charge field. Given that, in practice, the centre portion of the gaussian distribution is removed (see §2*e*) and that the magnitude of the space–charge field will, in any case, be smaller over most of the charge disk than it is at the edges, we can be confident that space–charge effects were negligible for the measurements in question.

(*b*) *The experimental cell*

The principal components of the experimental cell are sketched in figure 6. The cylindrical outer wall a and its top ring b were made of stainless steel; the lid c and bottom d of the cell were of copper. The ions were injected into the sample e of He II from a symmetrically placed array of seven tungsten field-emission tips f, each of which was spot-welded to a nickel shank that was held by a grub-screw (not shown) into a nylon holder g. The four grid-carrying electrodes h, i, j and k were all made of copper. Ions that passed through the gate formed by grids G_1, G_2 and G_3 entered the drift space between G_3 and the screening grid G_4 where a uniform electric field was maintained by suitable potentials applied to the copper

PHILOSOPHICAL TRANSACTIONS OF THE ROYAL SOCIETY A MATHEMATICAL, PHYSICAL & ENGINEERING SCIENCES

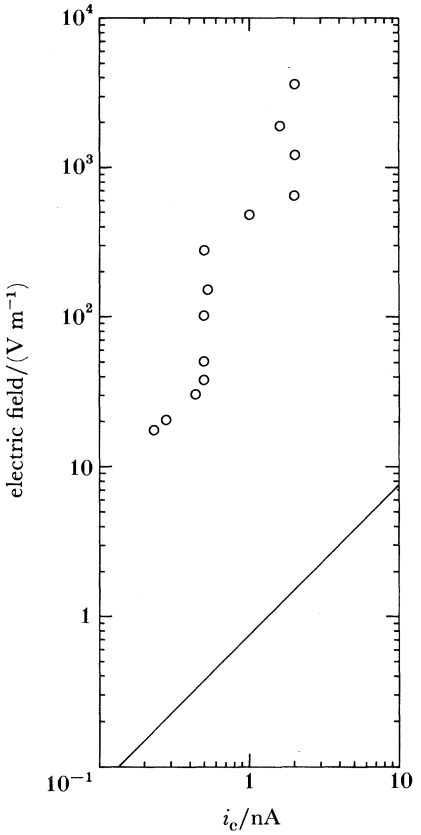

FIGURE 5. Relation between the electric fields in the drift space and the maximum signal current measured at the collector i_c. The solid line shows the space–charge field, calculated as described in the text, and the circled points indicate the applied electric fields at which some typical ionic velocity measurements were made.

field-homogenizing electrodes l. Finally, passing through G_4, they induced a signal in the collecting electrode m and were detected. The entire electrode structure was fixed to the lid c of the cell, which also carried the metal–glass seals (not shown) to admit electrical connections and the bushes for the sample-filling tubes (also not shown). An indium O-ring was used to provide the necessary seal between the top ring b of the chamber body and the lid c. The lid was secured by a ring of 30 M6 high-tensile stainless steel bolts, capable of withstanding the force of *ca.* 3 tonnes acting on it when the cell was at its maximum working pressure of 25 bar.

The four grids (200 lines/in†) were made of electro-formed copper mesh to match the thermal expansivity of the electrodes that carried them. A special stretching machine was used to tighten each grid to its yield point and it was then attached to its carrier with silver conducting paint. The grid and silver paint were then covered with an evaporated layer of gold to avoid any formation of insulating layers of oxide. The other electrodes were all gold-plated (in an electrolytic bath) for the same reason. The electrodes were separated from each other and from the body of the cell by nylon spacers but the cell geometry was designed in such a way, in particular by an overlapping of the homogenizing electrodes, that no insulator at all was 'visible' to ions within the drift space.

† 1 in = 2.54×10^{-2} m.

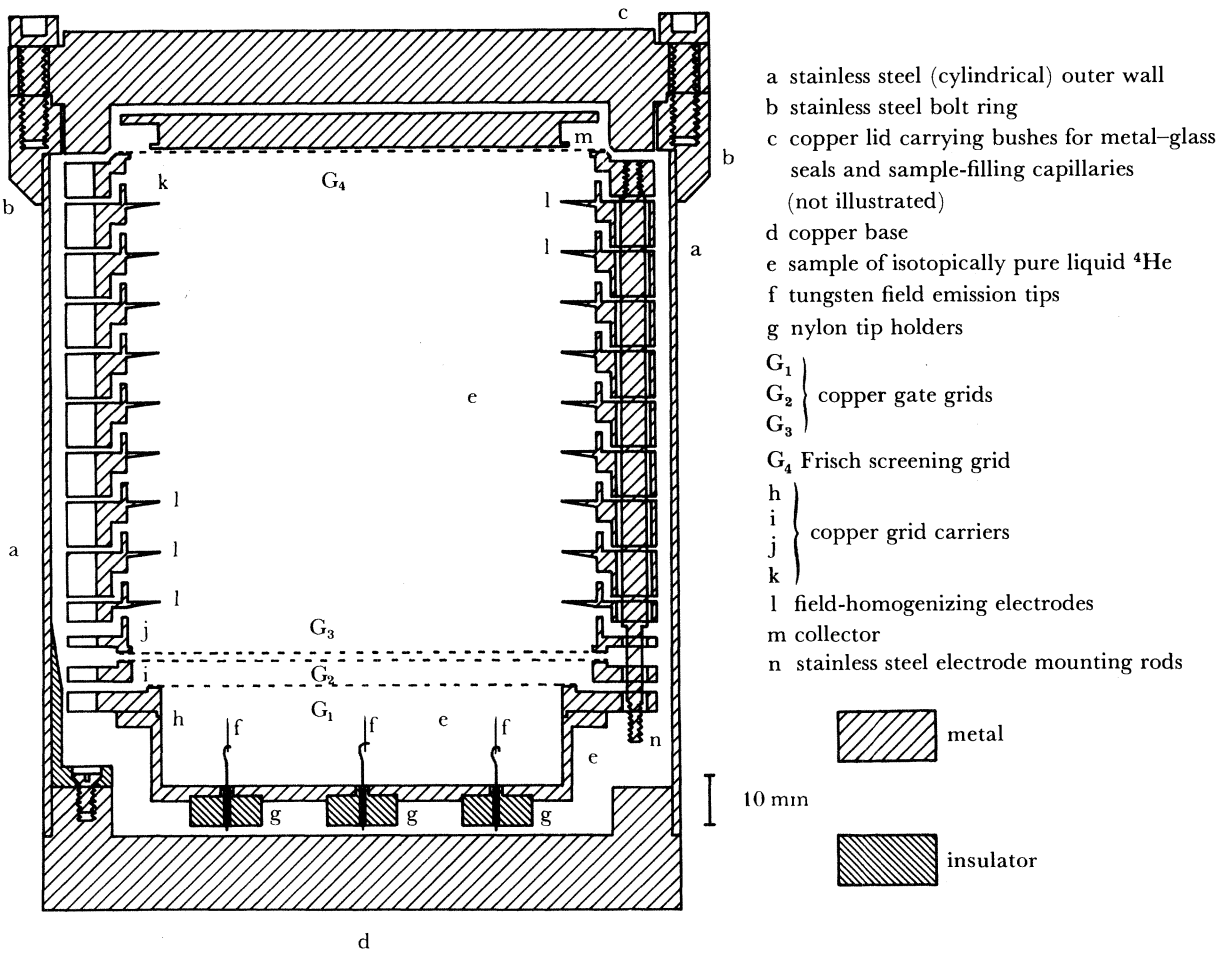

FIGURE 6. Sketch (not a section) showing the principal components of the experimental cell.

The most important dimension of the cell, the length, L, of the drift space specified by the separation of G_3 and G_4 was determined by four stainless steel mounting rods, n, onto which electrodes were threaded as sketched in figure 7. The precise details of the arrangement are extremely important because of the need to make proper allowance for the effects of thermal contraction. In the earlier measurements of I and II, a substantial fraction of the length of the cell was taken up by nylon, so that the amount of thermal contraction was both relatively large and also difficult to calculate with any confidence. Uncertainties in the cold length L consequently provided the major source of systematic error in those experiments. The present arrangement has been designed specifically to obviate these problems. The electrodes are insulated from each other and from the stainless steel rods n by nylon washers, but in such a way that the nylon plays almost no role in the determination of the G_3G_4 separation. One end of each rod screws into the grid carrier k that holds G_4. The grid carrier j holding G_3 is held firmly against a shoulder in the rod and is separated from it only by a steel washer p and a thin nylon insulating washer q. The precise spacings of the electrodes below j are, of course, much less critical and are determined by a series of nylon insulators r. A nut t acting via a spring washer s holds the whole electrode assembly tightly together on the rod at room temperature and, in particular, ensures that components p, q and j are held firmly against the

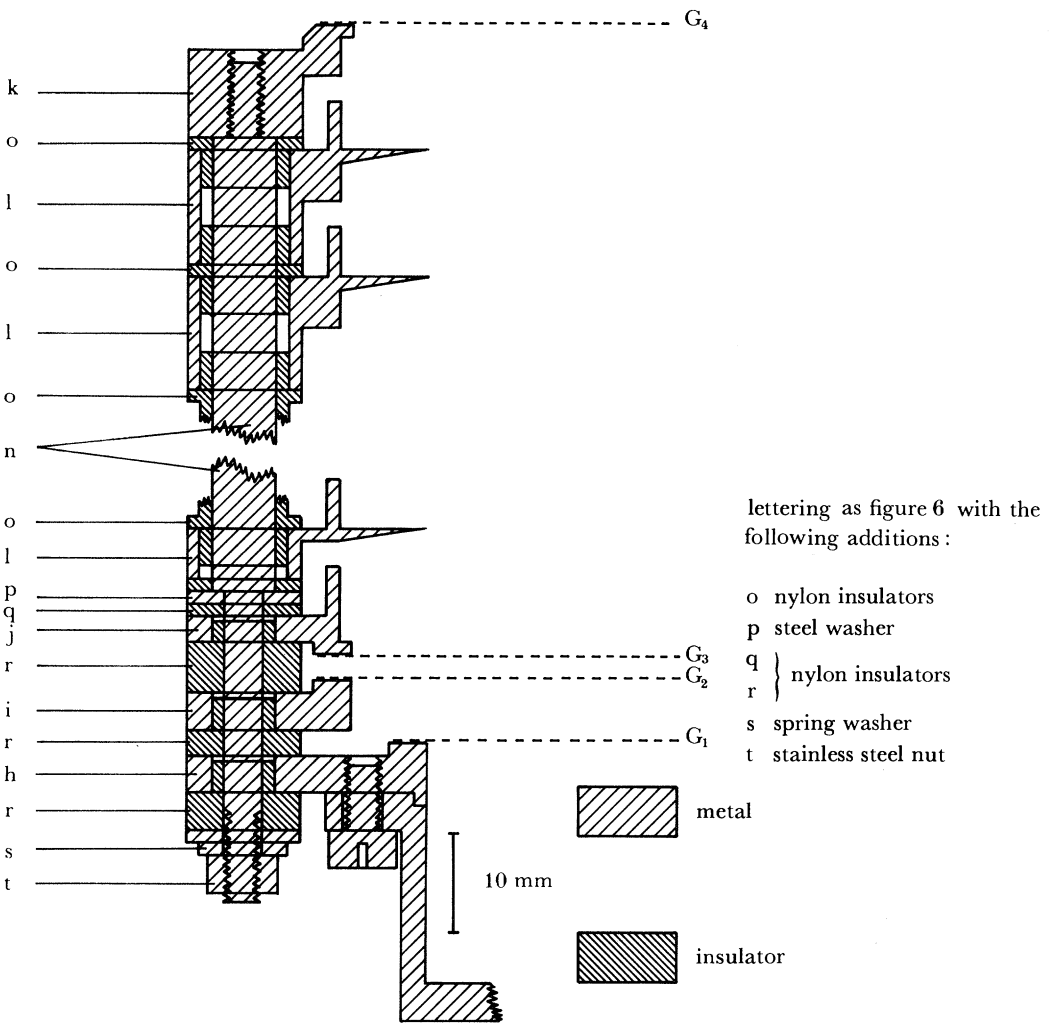

FIGURE 7. Radial section through outer rim of the assembled electrode structure. The structure is designed so that its axial thermal contraction will be very closely equal to that of the stainless steel mounting rod, n.

shoulder in n. When the cell is cooled, all its components contract, with the nylon ones contracting by a proportion that is about ten times larger than for the metal ones. Thus, the nylon spacers o tighten onto the rod n, but they have no reason to move along it, and the homogenizing electrodes l therefore remain in essentially the same positions on the rod. Because the nylon washer q is of negligible thickness compared with the length of the rod, its contraction can be ignored and we may assume that, to an excellent approximation, the thermal contraction in the length of the electrode structure is exactly the same as it would be if the whole assembly were constructed of the same type of stainless steel as the rods in n: that is, about 0.3 % between room temperature and the operating temperature.

Except at the points where the electrodes passed over the rods, there was a surplus copper that was carefully trimmed away as indicated on the left-hand side of figure 6. This had the dual effect of lightening the assembly and of providing spaces in which the electrical connections could be completed. The open-work nature of the whole structure facilitated thermal contact between the helium in the drift space and the copper lid of the chamber through which it was cooled.

The separation of G_3 and G_4 was determined in two different ways. First, it was calculated from measurements of individual cell components before assembly and secondly, it was determined by direct measurement of the assembled electrode structure through use of a travelling microscope. The two values agreed within experimental error, the latter being the more accurate. It is, of course, inevitable that the grids will sag very slightly under gravity. We have not in fact attempted to measure the magnitude of this effect. However, given that G_3 and G_4 are of equal diameter, that they are both made of copper and mounted on copper substrates, and that they were both stretched to the same tension (the yield point) during assembly, it seems reasonable to suppose that they will each sag by the same small amount and that L will therefore be unaffected.

Assuming that the stainless steel mounting rod (n in figure 7) contracted by 0.3 % between room temperature and 80 mK, we conclude that the cold length of the drift space is $L = (100.3 \pm 0.2)$ mm.

(*c*) *Electrical circuitry*

In figure 8 we show a block diagram of the electrical circuitry used for the experiments. The arrangement can be divided into two parts. Above the cell is shown the apparatus used for producing and measuring the various pulses applied to the electrodes. Below the cell are shown the components used to provide the appropriate d.c. bias voltages.

The central feature in the circuit is the Nicolet 1280 minicomputer, which acts as the master trigger source and creates the gate pulses, as well as providing all the computing power needed for the signal analysis after completion of averaging. The trigger from the computer initiates the tip pulse and simultaneously starts a signal sweep in the Nicolet analogue to digital converter (a.d.c.). The gate pulses are provided from the computer's t.t.l. (transistor–transistor logic) output, this being quite sufficient (± 5 volts) to operate the gates in the cell. The trigger and gate pulse are both software controlled and were found to provide a very stable timing source. The computer has a hard disk storage system that was used to store the raw data together with the results of the analysis. The digital graph plotter, also part of the computer system, presented the data graphically immediately after completion of analysis.

Once the d.c. biasing of the cell had been adjusted, it was left unchanged and only the drift-field voltage was varied while making a set of velocity measurements. A digital voltmeter was connected directly across the drift space between the third and fourth grids to monitor their potential difference V_d, which could lie anywhere within the range $2\ \text{V} < V_d < 400\ \text{V}$. The ion signals of *ca.* 1 nA reaching the collector were amplified by a Keithley 427 current amplifier with a minimum nominal risetime of 10 μs, before being averaged to enhance signal:noise.

The tip-pulse shape was formed at low voltage in a home-made pulse shaper, and then fed to the input of a Fluke 5205A precision power amplifier. This provided a voltage amplification factor of 100 with a bandwidth from d.c. to 100 kHz and a maximum output rating of 200 mA at 1.5 kV.

All the d.c. biasing for the cell was derived from batteries to eliminate possible 50 Hz interference and earthing problems associated with mains power sources. B1 and B2 were both 6 V batteries that biased (open) the spaces between the first and second grids and between the second and third grids respectively. The bias voltages could be set to their required values by adjustment of VR1 and VR2 for optimum electric field within the gate. The problem of field mis-match across individual grids is discussed in §2*h*.

The gating pulse, which is a positive pulse applied to the second grid, is sufficient to reverse

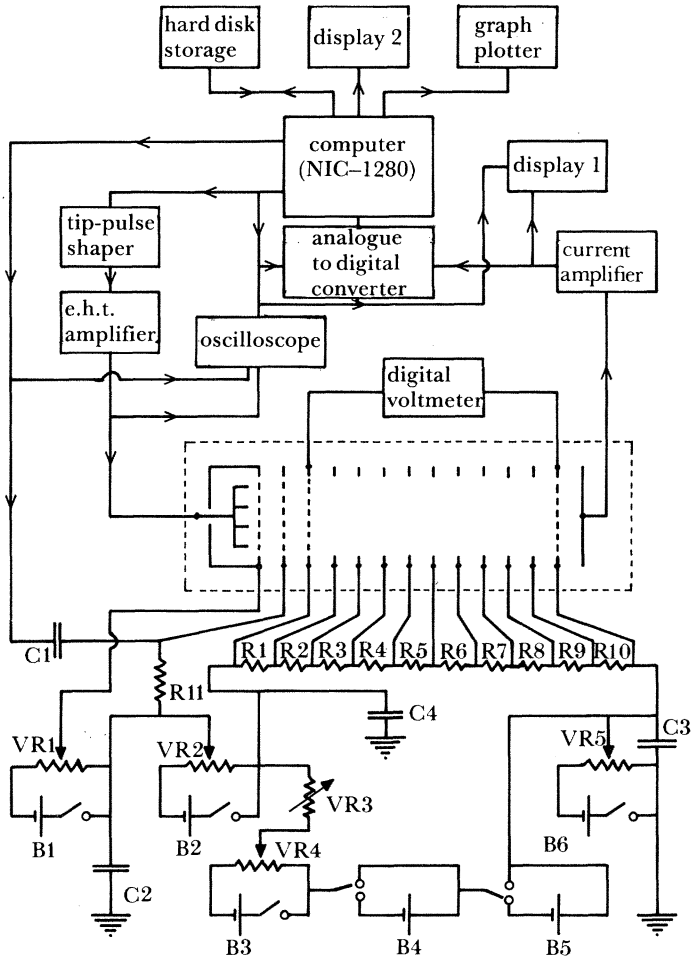

FIGURE 8. Block diagram of the electrical circuitry used for the measurements. The components inside the broken line represent the electrodes of the experimental cell, operating in isotopically pure liquid ^{4}He at *ca.* 80 m K. All other components are at room temperature.

the field between the second and third grids. This pulse is fed to the cell via the capacitor C1 that, with R11, has an *RC* time constant of *ca.* 1 s, so that there is no significant droop on the gating pulses. The decoupling capacitors C2, C3 and C4 provide low impedance a.c. paths to earth, so that no voltage pulses appear across the drift space.

The batteries B3, B4 and B5 were usually of 90 V each (although additional batteries were sometimes also used) and provided the drift field. The voltage could be adjusted by means of VR3, VR4 and the switches in series, and it was applied across a series chain of ten 100 K high-stability resistors. This gave a uniform voltage drop down the length of the drift space when applied to the field-homogenizing electrodes inside the cell. Finally, the battery B6 gave a bias of up to 6 V to the fourth (Frisch) grid, relative to earth and to the collector.

(*d*) *Cryogenics and gas handling*

The ionic cell with its charge of $1\frac{1}{2}$ litres of isotopically pure liquid ^{4}He at 25 bar was cooled to below 0.1 K by using a cryostat that had started life as a commercial Oxford Instruments dilution refrigerator. The original construction was modified extensively to accommodate the very large cell with its sample-filling lines.

The modified dilution refrigerator was a simple one, comprising a still, a concentric-tube heat exchanger and a mixing chamber, to which the cell was attached. Considerable care was taken to minimize heat leaks through the sample-filling capillaries. As can be seen from figure 9, there are two pressure filling lines to the cell. Both of these were passed down the inside of the concentric-tube heat exchanger as well as looping the still and the 1 K pot and forming another heat exchanger in the main helium bath. The need to limit the thermal flux into the mixing chamber meant that, below the still, the tubing had to be kept to a minimum diameter. The tubes that enter the cell were of 0.5 mm outer diameter, 0.3 mm inner diameter and made of cupro-nickel; each of them ran for a total length of *ca.* 1 m through the heat exchanger and up to the still. The copper top of the cell was rigidly bolted to the mixing chamber by four threaded copper rods, to provide thermal contact. Thermometry was by means of a pre-calibrated germanium resistor thermally anchored to the mixing chamber. Its resistance was measured by use of a four-terminal d.c. technique and the temperatures determined in this way were used in the calibration of carbon thermometers whose resistance could more conveniently be measured through use of a conventional a.c. Wheatstone bridge.

By using this arrangement, it was possible to fill the sample of *ca.* $1\frac{1}{2}$ litres of liquid in a little over a day. The gas was condensed into the cell while the refrigerator was running, at such a rate that the mixing chamber did not warm up appreciably, thereby keeping the cell at 0.1 K or so.

As shown in figure 9, the isotopically pure ^{4}He gas was passed through a series of liquid-nitrogen-cooled charcoal cleaners before condensation, to remove any traces of air or other forms of contamination. The system of valves around the traps in conjunction with the helium 'bomb' was used to flush the cell at room temperature. It was desirable to remove as much of the air in the cell as possible, after it had been connected to the system. This was necessary for two reasons; first, to prevent any blockage of the filling lines with solid air (which happens all too easily in $\frac{1}{2}$ mm tubing); and second, to minimize any adsorption of air onto the grids and field-homogenizing electrodes inside the cell. The narrowness of the tubing prevented effective pumping of the cell, so a flushing system was essential. The procedure was to condense isotopically pure ^{4}He gas into the bomb at 4 K. This helium could then be used to pressurize the cell via the traps, typically to 20 bar if the bomb was raised to room temperature to expel its contents. Lowering the 'bomb' to 4 K, the helium could once again be condensed into it, via the trap, but this time from the cell. This flushing procedure was used half a dozen times, cycling the pressure between 20 and 1 bar on each occasion.

The gas was always condensed down just one tube, with the second tube acting as a safety device in case a blockage occurred in the first tube. The second tube was connected to a Texas Instruments pressure gauge. This arrangement had the advantage that the gauge in question always gave a true indication of the actual pressure in the cell, because it was not connected directly to the condensing line. The Texas gauge was calibrated to a high precision and it was used throughout the experiments as the absolute pressure indicator.

(*e*) *Velocity measurements*

The operating procedure for making velocity measurements was as follows. The computer initiated a data sweep and triggered a high-voltage negative pulse (*ca.* -1500 V; see figure 10), which was applied to the field-emission tips at the left end of the cell (figure 8). This caused the tips to emit ions into the space between the tips and the first grid. The tip potential, V_t, was then kept at a very much smaller negative value but still below the potential of the first

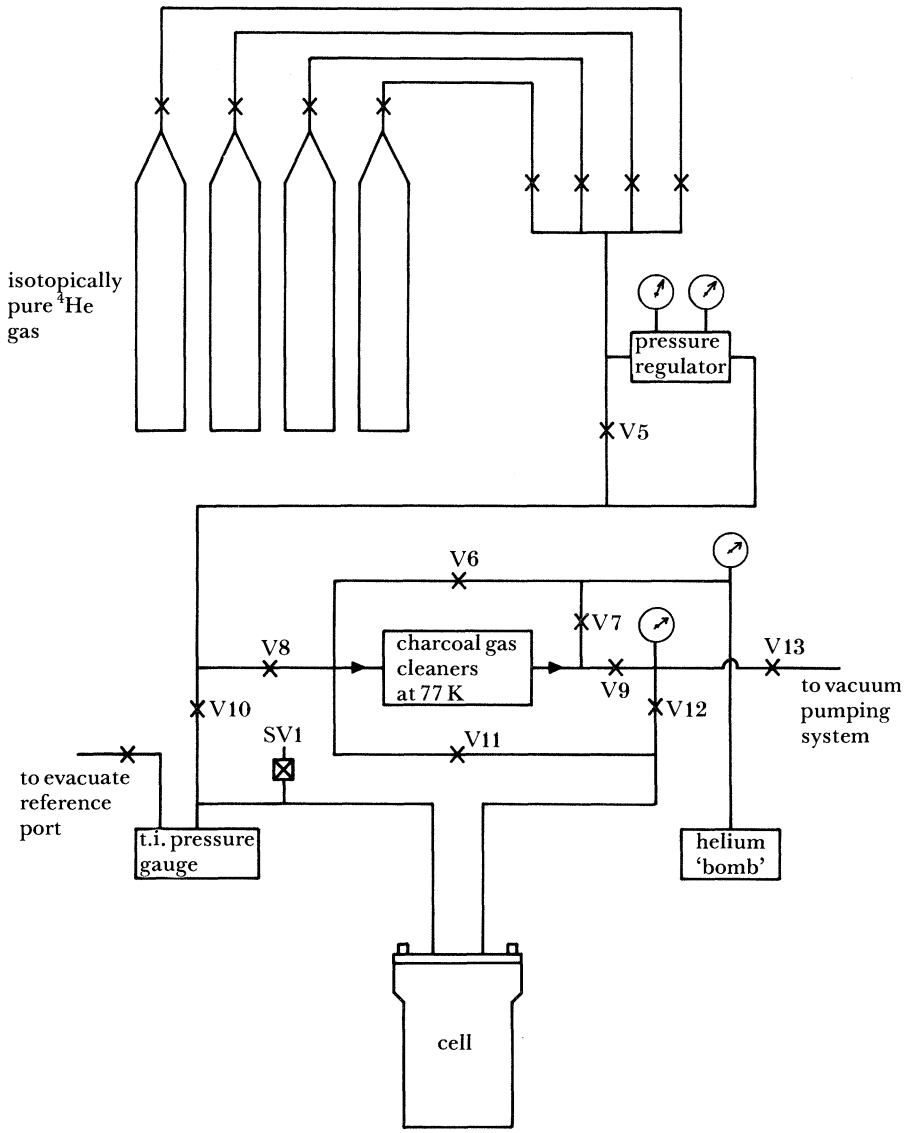

FIGURE 9. Simplified schematic diagram of the gas-handling system for the isotopically pure ^{4}He.

grid, so that the ion pulse progressed to and penetrated the gating system. This tailored-tip pulse is shown in figure 10*a* and is the first of the pulses applied to the cell. It can be seen that it is not a simple negative pulse and a detailed consideration of the reasons for the particular shape used is given in §3*a*.

The d.c. bias voltages on the first three grids were such that they were normally held open to the ion pulse. To make the measurements of drift time, a positive gating pulse was applied to the second grid such that the net field between the second and third grids was reversed and the gate thereby closed. At the end of the gating pulse the gates returned to the open state and the ions could enter the drift space. The gate pulse is shown in figure 10*b*; it was applied to the gates after the emission phase of the tip pulse had finished, being timed to occur soon after the arrival of the ion pulse at the gate. The net result was that the ion pulse had a hole 'burnt' into it at a precisely defined time.

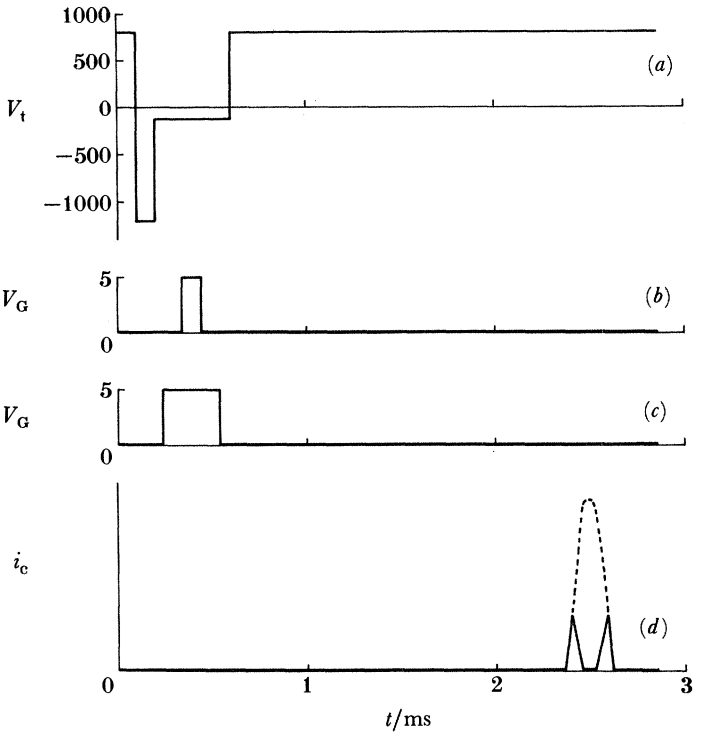

FIGURE 10. Sketches of voltage pulses applied to the cell and of signals induced in the collector, plotted in each case as a function of time t. (*a*) Typical form of the high-voltage pulse V_t applied to the field-emission tips. When resting, between emission events, the tips are maintained at a positive potential with respect to G_1 (see figure 6). A brief (*ca.* 100 μs) negative pulse is applied to induce field-emission of ions into the liquid; this is followed by a period of *ca.* 400 μs when the emitters are kept at a small negative potential to assist bare ions in penetrating G_1 and finally, the tips return to their positive resting potential. (*b*) A positive voltage pulse of magnitude $V_G = 5$ V and duration *ca.* 40 μs applied to G_2 (see figure 6) can be used to close the gate formed by G_2 and G_3. (*c*) A wider positive pulse, appropriately timed, can be used to ensure that none of the ions is able to reach the collector. In the acquisition technique normally employed (see text) narrow and wide gate pulses were used alternately to eliminate coherent noise on the signals. (*d*) Sketch to show the form of the signal expected at the collector. The collector current i_c is plotted as a function of time. If gate pulses are being applied, the centre of the signal is removed in a precisely defined manner to yield a twin-peaked signal as shown by the full line. The broken curve indicates the typical shape of the signal in the absence of a gating pulse.

After being gated, the ion pulse drifted the length of the cell under the influence of the drift field due to the voltage applied between the third and fourth grids, eventually giving rise to a signal in the collector as sketched in figure 10*d*. After amplification, the signal was passed to the computer for signal averaging, analysis and finally storage on hard disk.

The Nicolet a.d.c. (which in fact is an internal subsystem of the computer although, in the interests of clarity, it is shown as a separate box in figure 8) provided a 20 MHz eight-bit digitizing facility. Each sweep filled 8 K of memory locations. With a dwell time for each digitization of 0.5 μs, this gave a total sweep time of some 4 ms. The number of sweeps averaged in each case was determined by the required signal:noise ratio, which in turn was determined by the type of measurement being made; that is, either an absolute velocity measurement (see §2*f*) or a relative one with the use of cross-correlation techniques (see §2*g*).

The conventional signal-averaging technique proved quite adequate for the removal of random noise from the signal (the current amplifier noise of 1 nA being of the same order of

magnitude as the signal itself). However, there was a residual noise source which, although much smaller than the random noise, was coherent with the signal and therefore did not average away. To surmount this limitation on the final signal quality, the following modified signal-averaging process was used.

After every sweep the 8 K of acquisition memory was inverted (multiplied by -1) and with every alternate sweep, the gating pulse was widened sufficiently (figure 10*c*) to blank the signal out entirely for that sweep. The result was that every sweep was subtracted from the last, removing any coherent noise from the final average. Because the ion signal was gated out during every other sweep, it was not subtracted from itself. Although this process reduced the efficiency of the averaging as a means of removing the random noise, this was more than compensated by the almost total elimination of the coherent background. It was usually possible to increase the number of sweeps, without taking too much time, to retrieve the original random noise elimination. The fact that the whole acquisition process and gating system were under software control made the system both versatile and extremely stable. The only slight drawback to the inverting acquisition was the necessity of inverting the whole of data memory after every sweep. This was rather time-consuming and limited the maximum acquisition rate to *ca.* 4 Hz. This was, however, entirely reasonable for the particular circumstances of the present measurements.

The process outlined above was general to almost all of our data acquisition. The next two sections outline the different modes of analysis of the signal-averaged data for extraction of the ionic velocities.

(*f*) *Absolute measurements*

The action of the gate in closing and then re-opening is to 'burn' a hole in the otherwise rounded shape of the ion signal (figure 10*d*). The result is shown in an enlarged (and somewhat idealized) form in figure 11*a*. The two spikes sketched at the beginning of the sweep represent pick-up by the collector circuit of the gate shutting and opening transitions. The resultant ion transit times between various electrodes, from each of which $\bar{v}$ can (in principle) be calculated, are shown as $\tau_{s1}, \tau_{s2}, \tau_{01}$ and τ_{02}. The lengths in the cell corresponding to these times are readily appreciated by reference to the diagram of the electrode structure in figure 6. We will ignore, for now, the finite risetime of the collector circuit.

The time at which the signal first starts to rise is unrelated to the gate pulse, and corresponds to a velocity that is rather poorly defined because of the non-uniform electric field around the emission tips. The interval τ_{s1}, on the other hand, is precisely equal to the ionic transit time between G_3 and G_4. The time taken for the signal to fall to zero represents the time taken to cross from G_4 to the collector m, so that τ_{s2} corresponds to the G_3-to-collector transit time. When the gate opens again, the situation is a little more complicated. Provided that the gate remained closed long enough for all the ions that were caught between G_2 and G_3 to be drawn back to G_2, then τ_{01} and τ_{02} will represent the G_2-to-G_4 and G_2-to-collector transit times respectively. If the gate pulse were shorter than this, however, the significance of τ_{01} and τ_{02} would be poorly defined. The moment at which the signal finally falls to zero represents the transit time from f to m, with part of the passage through a region of non-uniform electric field and with no relation to the gate pulse.

The finite risetime of the collector circuit provides an added complication. In particular, it will have an especially serious effect on the sharpness of the point where the signal falls to zero for the first time and thus on the precision with which τ_{s2} can be measured. It will have a much

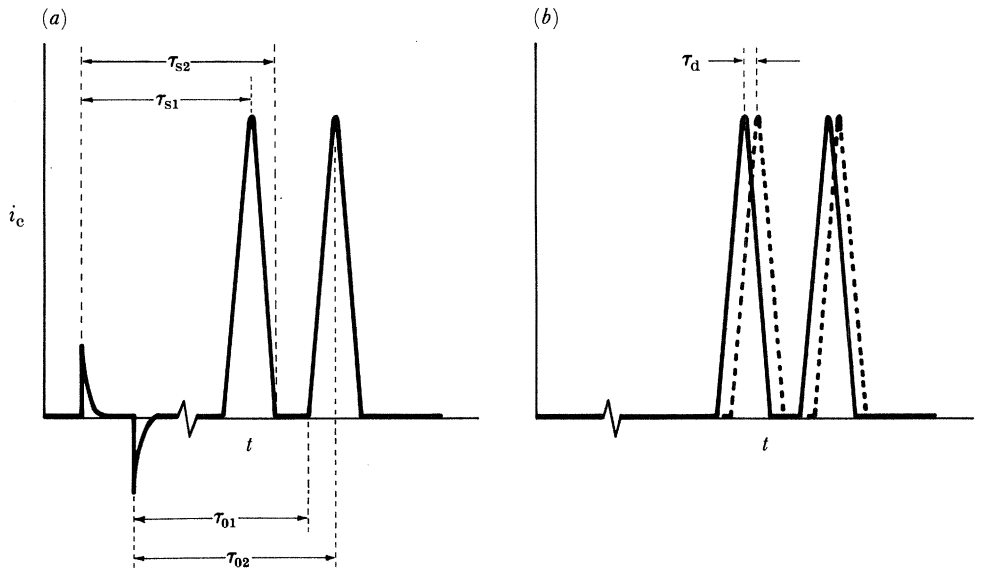

FIGURE 11. Sketches to illustrate the two chief techniques used for measurement of the ionic drift velocity. In each case, the collector current i_c is plotted as a function of time t and the portion of the abscissa corresponding to the transit of the ions between G_3 and G_4 (see figure 6) has largely been omitted. (*a*) For absolute velocity determination, measurements were made of the times τ_{s1} that elapsed between the gate-shutting transient and the corresponding point on the signal, as described in the text. (*b*) For relative velocity measurements, a cross-correlation technique was used to measure the delay τ_d between a reference signal (full curve) of known drift velocity and the signal (broken curve) whose velocity was to be determined.

smaller effect on the measurement of the other characteristic times in figure 11*a*. The use of τ_{01} or τ_{02} for measurement of $\bar{v}$ carries the disadvantage, however, that the relevant length includes the G_2G_3 space where the electric field will in general be different from that between G_3 and G_4. Furthermore, there is the added potential difficulty, already alluded to, that spurious results are very easily obtained in cases where the duration of the gate pulse is insufficient. In the light of these considerations, it is clear that the most satisfactory determination of $\bar{v}$ can be achieved through measurement of τ_{s1}; the corresponding length of G_3G_4 is well defined and accurately known; the length of the gate pulse is relatively unimportant and the effect of the finite risetime of the collector current and amplifier should be minimal. All of the velocity measurements to be presented rely, directly or indirectly, on the use of τ_{s1}.

It is now necessary to consider in rather more detail the shape to be expected of the signal $i_c(t)$ in the vicinity of the first peak, so that we can appreciate how best to determine the point corresponding to the moment at which the near edge of the front section of the ion pulse passes through G_4. In the equivalent situation during the experiments of I and II, we fitted straight lines to the adjacent regions of the signal and then computed their point of intersection. The present experiments differ in one important detail, however, in that the density of ions in the group entering the drift space is changing rapidly with time (whereas, in the earlier work, the emission current was allowed to equilibriate before ions were admitted to the drift space). Consequently, it is no longer appropriate to model the gated section of the signal with a series of straight lines, even if one were to ignore the rounding introduced by the finite risetime of the collector circuit.

In practice, the lengths of the gate pulse and the tip pulse, and the timing of the former

relative to the latter, are adjusted so that the points on the signal corresponding to the gate shutting and opening both fall in regions where i_c is respectively rising or falling in a sense approximately linear with t. Thus, the charge density in the travelling group of ions is axially inhomogeneous and must vary linearly with position along the cell at any given instant. At the moment when the rear of the first section of the plug of ions passes G_4, at a time τ_{s1} after the gate-shutting transition (figure 11), the charge density at G_4 is considerably larger than that at the collector m (figure 6). As a result, the fall in i_c as ions are collected in m (and not replaced by more ions entering through G_4) proceeds more slowly than would be so if the charge density were uniform: the resultant decrease in i_c is therefore nonlinear. By using the ideas in §2 of III and on the assumption of a linear variation of charge density with position, it is straightforward to show that $i_c(t)$ will be a quadratic of the form

$$i_c = a + bt - ct^2, \tag{2.1}$$

where a, b and c are positive constants. We conclude, therefore, that in modelling $i_c(t)$ in the vicinity of the first peak in the ion signal, it will be appropriate to fit a straight line to the data to the left of the peak, and a quadratic of the form of (2.1) to the right of the peak. The effect of the finite risetime of the collector circuit will be relatively small at this point and can be considered to be subsumed in (2.1) through a suitable small adjustment to the values of a, b and c.

The analysis programme exhibited the averaged data on display number 2 (figure 8), with four electronic cursors superimposed which could be positioned at any chosen point on the signal. One pair of cursors was used to define a region to which a straight line could be fitted on the left of the peak; the other pair of cursors was used to define a region just to the right of the peak to which (2.1) could be fitted. In each case, a least-squares procedure was used to perform the fitting. The intersection of the two fitted lines was then computed. The cursors could also be positioned to locate the transients corresponding to the gate transitions. Thus τ_{s1} could be computed and hence, by dividing it into the measured G_3G_4 separation, the ionic drift velocity $\bar{v}$.

As a general check on the consistency of the technique, we have also determined $\bar{v}$ from measurements of τ_{s2}, τ_{01} and τ_{02}. These were made in a similar way to that of τ_{s1}, by using a least-squares method to fit lines to appropriate regions of the signal in each case. By using the measured G_2G_3 and G_4 m spacings of 2.5 and 1.0 mm respectively, allowing for the fact that the electric fields between G_2 and G_3 and between G_4 and m differed from the field in the drift space between G_3 and G_4 and making an appropriate correction (Schwarz 1972) to take account of the finite time constant of the amplifier and collector circuit in the case of τ_{s2}, we have found agreement to well within the experimental uncertainty of *ca.* 0.5 % for velocities determined in these different ways. As already mentioned, however, we consider the values of $\bar{v}$ derived from τ_{s1} to be more accurate and reliable.

In practice, the alternative acquisition technique used for removal of coherent noise on the signals also had the effect of introducing ambiguities into the transients at the beginning of the signal (three from the tip and four in total from the gate). For this reason, the positions of the (narrow) gate transients were in fact determined occasionally by the passing of a few sweeps of the gate signal directly into the a.d.c. and the determination of the transition times by means of the cursor display. Because all times in the experiment were derived from the

computer, the gate position was very stable over long periods of time and never shifted more than one channel (0.5 μs).

For the absolute velocity measurements, the quality of the final signal was of particular importance because of the need to fit lines to the sides of the first peak (see above). For this reason, the gain of the current amplifier was set to a smaller value (10^7 V A^{-1}) than that (10^8 V A^{-1}) used for the relative velocity measurements described in the next section. The lower range reduced the distortion of the signal caused by the finite risetime of the amplifier and collector circuit, but had an adverse effect on the signal: noise ratio. The latter quantity can, however, in principle always be improved by an increase in the number of sweeps, N, in the average. In practice N varied from 4000, which was found adequate for data acquired at pressures above *ca.* 17 bar, up to 20000 at 13 bar, where the signal became extremely weak.

(*g*) *Cross-correlation methods*

The bulk of our velocity measurements were not made as described in §2*f*, but were in fact relative velocity measurements: the measurement in each case was of a velocity change from a known reference point. The general operating procedure for data acquisition was essentially the same as for the absolute velocity measurements previously discussed; the mode of analysis of the signal, however, was entirely different.

First of all a reference data point was taken at a value of drift field where the absolute velocity was known, that is, under conditions where we had already made an absolute velocity measurement as described above. The drift field was then changed and another ion signal averaged. Figure 11*b* sketches two such signals superimposed. The important quantity is the displacement τ_d of the data signal from the reference signal. Once this quantity is known, it is simple to find the new velocity. The relative velocity-analysis routine performs a cross-correlation between these two signals. The resulting cross-correlation function will have a definite maximum. If there is a zero time-difference between the reference and the data signal, then the correlation function is centrally placed. Any finite τ_d will result in a similar but shifted correlation function, the displacement from the mid-position being a direct measurement of τ_d.

The advantage in using a cross-correlation analysis is that the whole of the signal is used in calculating the cross-correlation function and this can give a substantial improvement in precision. Even with quite noisy data, the cross-correlation function is relatively smooth, as we shall see in §3*a*. This can be appreciated from the fact that white noise cross-correlated with white noise gives a zero result. Experimentally, it was found possible to degrade the signal: noise ratio appreciably, without altering the cross-correlation result. This meant that it was possible to use considerably smaller numbers of sweeps in many data averages, a few hundred often being quite sufficient.

In the data analysed, the gating of the signal gives rise to additional structure in the cross-correlation function, with two smaller peaks appearing, one on either side of the principal maximum. Because the gating position is very stable, this additional sharpness in the cross-correlation function gives improved accuracy. The actual signal shape can, of course, be of any form, so long as it remains the same for the signal and reference signal. This meant that signal-distortion was quite unimportant and the gain of the current amplifier could therefore be set to optimize the signal: noise ratio, notwithstanding the resultant extension of the risetime of the input circuit.

PHILOSOPHICAL TRANSACTIONS OF THE ROYAL SOCIETY A MATHEMATICAL, PHYSICAL & ENGINEERING SCIENCES

(*h*) *Transient voltage technique*

For low values of the drift-space electric field there is a problem of field mis-match between the field in the drift space and the gate region. Because the higher field usually exists inside the gate region a large proportion of the gate field-lines end on the wires of the grid. This means that ions, following the field lines, end up being collected by the grid. Therefore, as the drift-space field decreases, the ion signal is increasingly attenuated.

A second consideration under these conditions is the 'leakage' of the gate field into the drift space. This should only be a very small effect because the grid spacing is only *ca.* 0.1 mm and the leakage distance into the drift space should consequently be only of about this size.

A third consideration relates to Schwarz's (1972) observation that, quite independent of the field mis-match effect referred to above, ions can sometimes be exceedingly reluctant to penetrate grids under the influence of weak electric fields. The origins of this surprising effect remain unknown, although it seems plausible (see §4*c*) to suggest that it may be associated with vorticity pinned on the grid wires.

To overcome these problems (or potential problems) a technique was developed for putting a voltage pulse on the drift space such that the d.c. drift field was reduced to some chosen low value for the duration of the pulse, as sketched in figure 12. To do this, the electrical circuit was slightly modified from that of figure 8, with a chain of capacitors and associated decoupling resistors being added to the drift-space electrode system. The timing of the pulse was such that it was initiated only when the ions had already entered the drift space and so that it ended before the ions had reached the screening grid. By using the correlation technique and comparing the signal without the drift pulse with the signal with the drift pulse, the delay could be found. Knowing the velocity for the relatively high-field condition and the duration of the field-reducing pulse, the low-field velocity could readily be calculated.

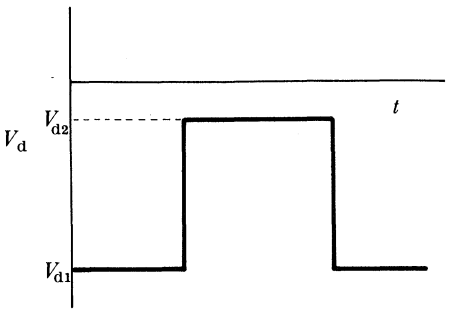

FIGURE 12. Sketch to show the form of the voltage pulse applied across the drift space for transient low electric field measurements. The drift-space potential difference V_d is plotted as a function of time, t. The ions passed G_3 (see figure 6) and entered the drift space while a relatively large negative voltage V_{d1} was being applied. While they were in transit between G_3 and G_4, the voltage was reduced to a smaller value of V_{d2}; but it was restored to its original value before they reached G_4.

3. EXPERIMENTAL RESULTS

(*a*) *Ion signals*

Figure 13*a*, plotting the collector current i_c as a function of time t, shows a typical (averaged) signal in its entirety, with $E = 2.0 \times 10^3$ V m^{-1} and $\phi = 10^8$ V A^{-1}. The initial transients in i_c arise from the combined effects of the three-level field emitter pulse, the gate pulse, and the

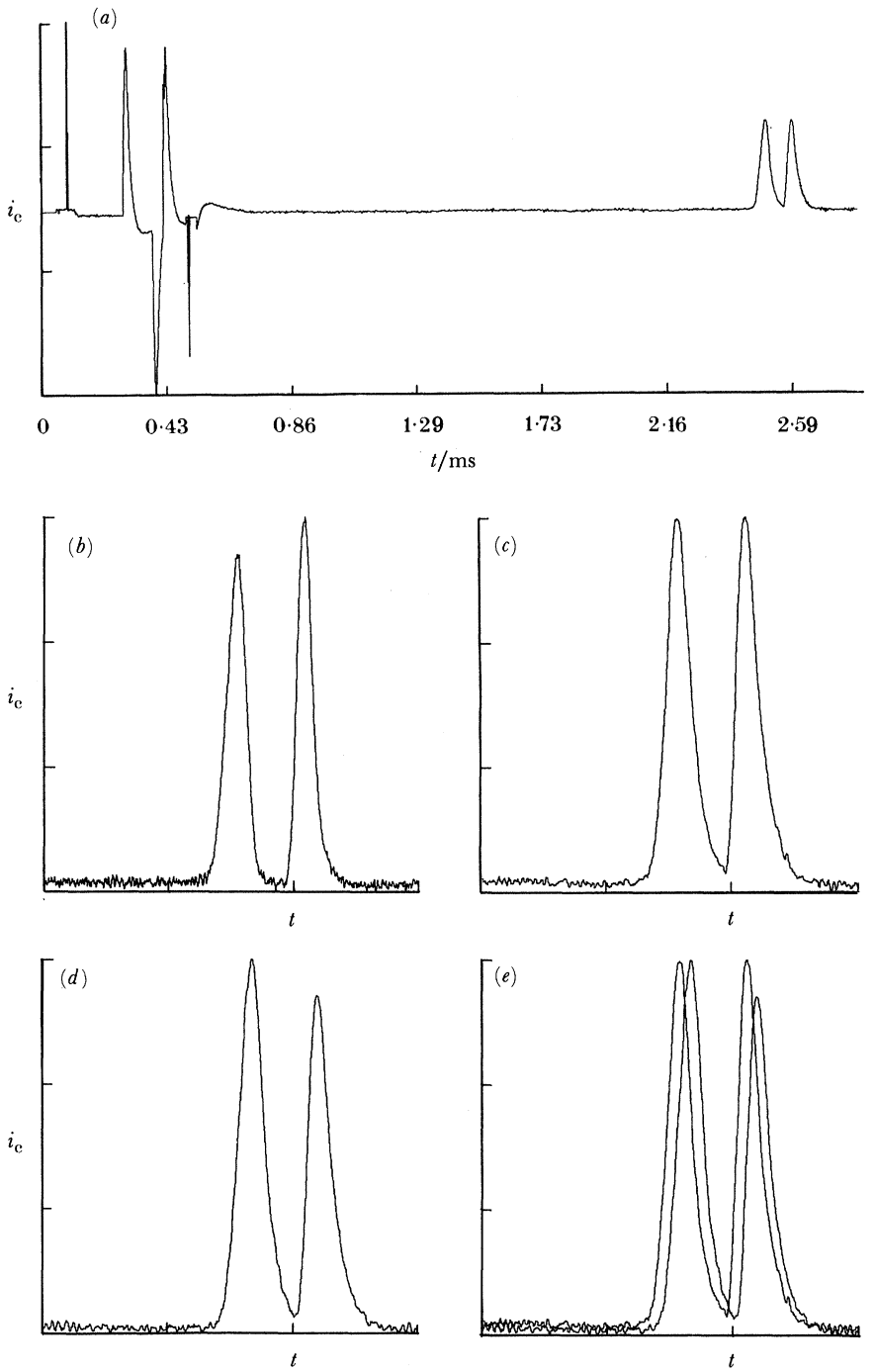

FIGURE 13. Examples of ion signals recorded at a pressure of 24 bar. In each case, the collector current i_c (in arbitrary units) is plotted as a function of time, t. (*a*) Complete a.d.c. sweep after averaging, showing the tip pulse and gating transients on the left-hand side and the twin-peaked ion pulse on the right, for an electric field $E = 2.0 \times 10^3$ V m^{-1}, an amplifier gain of $\phi = 10^8$ V A^{-1} and with $N = 1000$ sweeps in the average. (*b*) Ion signal, enlarged, with $E = 2.0 \times 10^3$ V m^{-1}, $\phi = 10^7$ V A^{-1} and $N = 4000$, suitable for an absolute measurement of the drift velocity $\bar{v}$, as described in §2*f*. (*c*) Signal with $E = 2.0 \times 10^3$ V m^{-1} as in (*b*), except that $\phi = 10^8$ V A^{-1} and $N = 1000$, suitable for measurement of changes in $\bar{v}$ by use of the cross-correlation method described in §2*g*. (*d*) Signal with $\phi = 10^8$ V A^{-1} as in (*c*) except that $E = 1.1 \times 10^3$ V m^{-1} and $N = 500$. (*e*) Superposition of the two signals shown in (*c*) and (*d*), to demonstrate the shift in arrival time.

blanking pulse applied to alternate signal sweeps (§2*c*). There follows a region of flat baseline and then the ion signal itself on the right-hand side of the figure, looking very similar in form to that expected (figures 10 and 11).

Figures 13*b*, *c*, *d*, *e* show the ion signals enlarged, with transients and most of the baseline omitted, under a variety of conditions. In (*b*) is shown an example of a signal recorded with the amplifier gain set to 10^7 V A^{-1}. The risetime of the collector circuit is relatively fast at this setting, but the signal is correspondingly rather noisy before averaging. The response is fast enough, in fact, for short regions of flat baseline to appear between the two peaks. Signals of this type have been used for making absolute velocity measurements of the ionic drift velocity as described in §2*f*. The signal in figure 13*c* was recorded under identical conditions to that in (*b*), except that the amplifier gain was set to 10^8 V A^{-1}. At this setting, the response is slower, the peaks are broadened, and the baseline between the peaks has disappeared. The signal : noise ratio is significantly larger, however, despite the reduced number of sweeps included in the average. Signals of this type are well suited for drift velocity measurements based on the cross-correlation technique described in §2*g*.

The signal in figure 13*d* was recorded for an electric field of 1.1×10^3 V m^{-1}, compared with 2.0×10^3 V m^{-1} in (*c*), but all other conditions were left unchanged. As a result, the signal in (*d*) is delayed slightly with respect to that in (*c*), but it retains almost exactly the same shape. (The relative magnitudes of the two peaks, however, are slightly different for the two signals. This quantity depends critically on the exact potentials and timings of the emitter tip pulse, which have evidently drifted slightly during the period of *ca.* 1 h that elapsed between the recording of the two signals. The effect of such drift on the measured velocities is found to be negligible.) The delay of signal (*d*) relative to (*c*) is demonstrated more clearly in figure 13*e*, where the two signals have been superimposed on each other. Measurement of this delay is effected by computation of the cross-correlation function of the two signals, which is plotted in figure 14. The displacement of the central maximum from the (broken) zero-time axis is equal to the delay and is readily measured digitally with the computer.

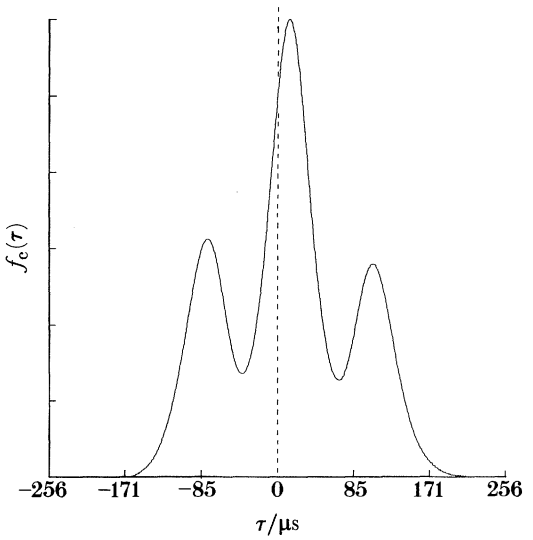

FIGURE 14. Cross-correlogram computed between signals (*c*) and (*d*) of figure 13. The cross-correlation function $f_c(\tau)$ is plotted as a function of the offset time τ between the two signals. The displacement of the central maximum from zero offset time (broken line) gives a direct measure of the extent to which the signal in (*d*) is delayed relative to that in (*c*).

The signals of figure 13 were all recorded at 24 bar, where vortex nucleation occurs at a minimal rate and the signals are consequently strong. At lower pressures, the signal:noise ratio is relatively poor, even after extended averaging. Some typical signals recorded at 13 bar are shown in figure 15*a*,*b*, representing respectively the reference signal (which thus corresponds to that in figure 13*c*) and the delayed signal (corresponding to 13*d*). It is interesting to note that, although the signals themselves are extremely noisy, being totally invisible on the oscilloscope screen before averaging, their cross-correlation function is nonetheless quite smooth (figure 16) so that the delay of the signal in (*b*) relative to that in (*a*) can still be determined to high precision.

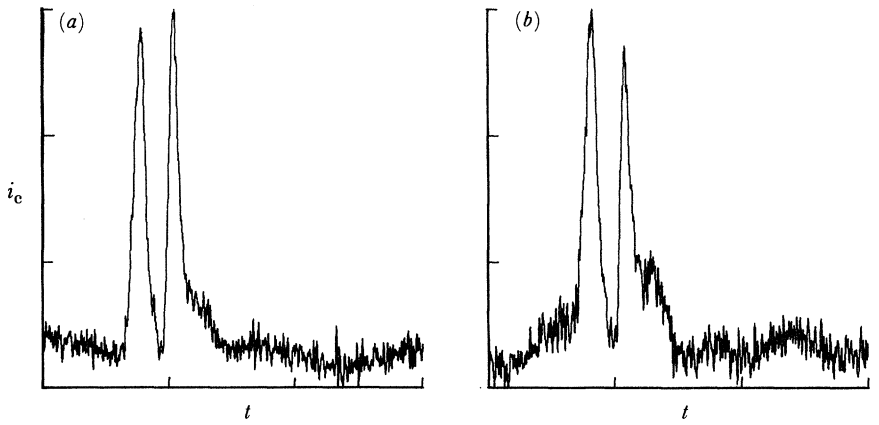

FIGURE 15. Examples of signals recorded at a pressure of 13 bar. In each case, the collector current i_c (in arbitrary units) is plotted as a function of time, t. (*a*) Ion signal for an electric field $E = 2.0 \times 10^3$ V m^{-1}, an amplifier gain $\phi = 10^8$ V A^{-1} and with $N = 6000$ sweeps in the average. (*b*) Signal as in (*a*) except that $E = 1\ 1 \times 10^3$ V m^{-1} and $N = 4000$.

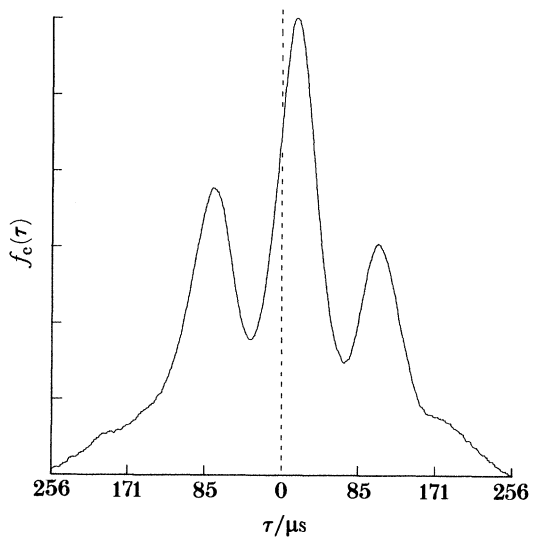

FIGURE 16. Cross correlogram computed between signals (*a*) and (*b*) of figure 15. The cross-correlation function $f_c(\tau)$ is plotted as a function of the offset time, τ, between the two signals. The displacement of the central maximum from zero offset time (broken line) gives a direct measure of the extent to which the signal in (*b*) is delayed relative to that in (*a*).

In fact, the cross correlograms are even smoother than figures 14 and 16 imply. In figure 17 we have plotted respectively in (*a*) and (*b*) the central portions of the maxima of figures 14 and 16, indicating the contents of each address in the computer memory as a discrete point. The curve for the 13 bar data (*b*) is broader at the peak than that for the 24 bar data (*a*) but otherwise there is little to choose between them. Given the smoothness of these curves, we have felt it justifiable to determine the position of the maximum in each case by parabolic interpolation, taking into the least-squares sums just the 6–10 data points on either side of the highest point. This means, in effect, that the precision with which we have been able to measure delay times is better than the inverse sampling rate (in this case, 0.5 μs per point) of the a.d.c. in the computer.

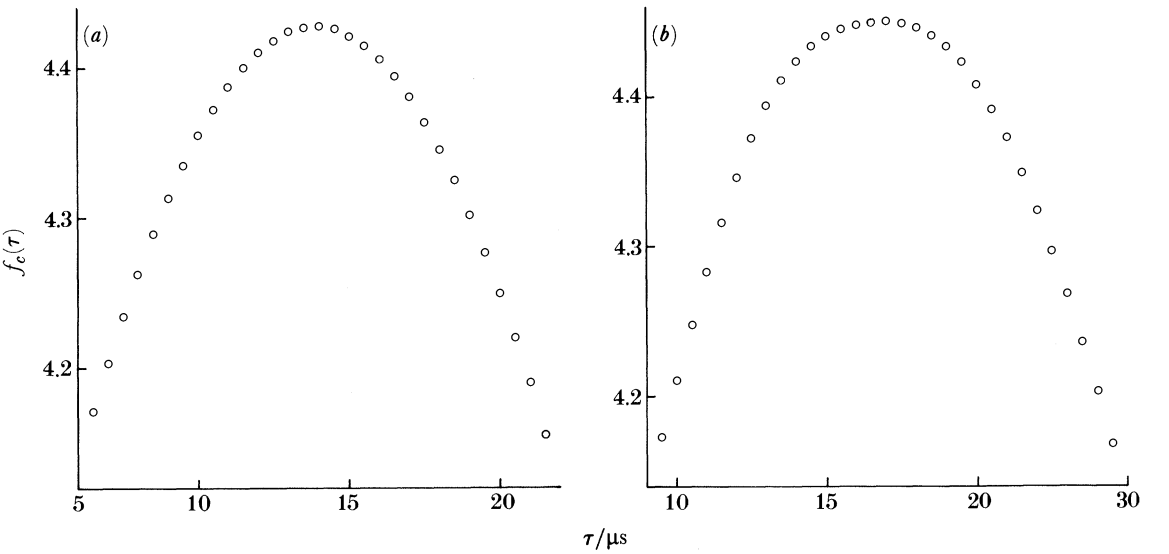

FIGURE 17. The central maxima of the cross correlograms of figures 14 and 16, greatly enlarged, are shown in (*a*) and (*b*) respectively. The number contained in each relevant computer address, multiplied by 10^{-5}, is plotted as a function of the offset time between the two signals in question. The space between the points, corresponding to the a.d.c. sample interval during data acquisition, is 0.5 μs. Parabolic interpolation gives the offset times of the maxima as 14.38 μs for (*a*) and 17.23 μs for (*b*).

The detailed shape of the signal in the vicinity of the first maximum in $i_c(t)$ is found to be very similar to that expected on the basis of the discussion above in §2*f*. In figure 18 we plot on a greatly expanded horizontal scale the first peak of a signal typical of those that we have used for absolute velocity measurements. Although the signal is rather noisy it is clear that, just to the left of the peak, $i_c(t)$ is approximately linear, whereas just to the right of the peak it shows a pronounced convex curvature attributable to the combined effects of the axial inhomogeneity of the ion cloud and the time constant of the amplifier input circuit.

It was found that the magnitude of the ion signal did not bear any simple relation to the size of the voltage pulse applied to the field emitters. Early on in the research programme, a single voltage pulse V_t was applied to the tips to initiate each sweep, and the tips were otherwise held at the same potential as that of G_1 and the backplate. Under these conditions and for a high pressure, a gradual increase in V_t resulted in an increase in i_c to begin with. Above a certain value of V_t, however, the signal disappeared abruptly. On reduction of V_t to a value where a large signal had previously been seen, the signal did not immediately reappear,

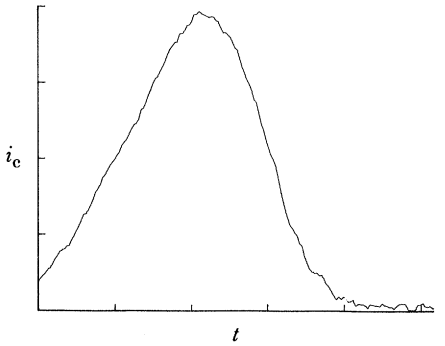

FIGURE 18. The collector current i_c, plotted as a function of time t. Each horizontal division corresponds to 32 μs.

although tip and gate were continuing to be pulsed at the usual repetition rate of 4 Hz. Rather, the signal returned gradually over a period of several minutes. The origin of this unexpected behaviour is not understood, but we may tentatively ascribe it to the increased production rate of vorticity when V_t is large, partly because the flux of ions from the tips is then larger and partly because the vortex nucleation rate (see II) increases rapidly with increasing electric field. It seems entirely possible for the helium near the emitters to become filled with a dense mass of vorticity as a result, either in the form of slowly moving rings or as a tangle of vortex lines produced by the mutual interaction of the rings. Some of this vorticity would doubtless find its way into the drift space, where it could conceivably affect the bare-ion signal in two different ways. First, if the vorticity were charged, it would distort the applied electric field, perhaps eliminating it on the axis of the cell or even reversing it, so that there would no longer be a force propelling the ions towards the collector. Second, the vortex lines could act as trapping centres for the ions which, again, would not be able to reach the collector. The experiments appear to favour the second of these alternatives because the growing signal, after reduction of V_t from an initial high value, did not appear to be distorted or anomalously slow but simply an attenuated version of what was measured under equilibrium conditions.

Unfortunately, it is not possible at the moment to make any reliable estimate of the vortex density in the cell to see whether the picture that we are tentatively proposing is a plausible one. We return to consider the problem again from a slightly different point of view in §4*c* below.

The size of the bare-ion signal arriving at the collector was strongly dependent on pressure. In figure 19, where we plot (circled points) the net charge

$$Q_c = \int_{\text{signal}} i_c \, dt$$

in each signal arriving at the collector as a function of the applied pressure, while keeping all other parameters constant, it can be seen that Q_c has fallen almost to zero by the time that the pressure has been reduced to 17 bar. Our initial measurements (Ellis *et al.* 1980*b*) were consequently restricted to the relatively narrow range of pressures within 19 bar $< P <$ 25 bar. Although the origin of this phenomenon is not understood in detail, it seems reasonable to attribute it, also, to the presence of vorticity; particularly given the very rapid increase in the vortex nucleation rate ν that is known (see III) to occur with decreasing pressure. The electric

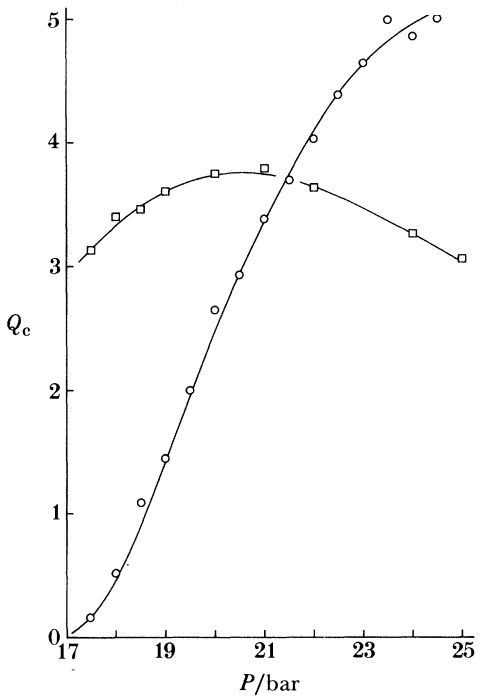

FIGURE 19. Pressure-dependence of the signal magnitude at the collector. The charge contained in the signal (arbitrary units) for a drift-space electric field of 715 V m^{-1} is plotted as a function of pressure P for a simple negative-going field-emission tip pulse (circled points) and for a tip pulse tailored (see figure 10*a*) such that the tips were held at a positive potential relative to G_1 (figure 6) during the resting periods between emission events (squares). The solid curves are guides to the eye. It should be noted that the absolute magnitudes of the two $Q_c(P)$ characteristics cannot be compared; in fact, that indicated by squared points was always considerably the larger and not just for the lower pressures.

fields existing in the drift space and between the gate grids are much too weak to cause significant vortex nucleation (except, of course, for pressures near 10 bar; see §2*a* above), so it may safely be assumed that most of the vortex nucleation events occur close to the field-emission tips during the brief period when they are being pulsed. Any charged vortex rings that are created may be expected to move away at a velocity that is approximately inversely proportional to their energy and very slowly indeed compared with bare ions, with many of them eventually entering the drift space and causing the complications discussed above. There is also a possibility that some of the rings may become tangled with each other, leading to a random tangle of charged vorticity surrounding the field-emission tips, thereby limiting the size of the electric field at the metal surface and hence reducing the emission current.

It was in an attempt to minimize the growth of vorticity around the emission tips that we introduced the carefully tailored emitter pulse shape discussed in §2*c*. The underlying philosophy is that the tips should normally be maintained at a potential positive with respect to G_1. To make them emit, a transient negative pulse of magnitude *ca.* −1.2 kV relative to G_1 and of duration *ca.* 100 μs is applied. To enable the ions so produced (or, at least, those ions which have not already metamorphosed to charged vortex rings) to pass through G_1, the tips are then kept at a small negative potential of *ca.* 100 V for *ca.* 400 μs and then, finally, they are returned to their 'resting' potential of *ca.* +500 V. The intention is to maintain a retarding electric field that will draw any charged vortex lines or rings away from G_1 and back

again towards the field emitters except, of course, during the brief episodes of ion injection. The results of this procedure were dramatic and are shown by the squares in figure 19. It can be seen immediately that the pressure dependence of Q_c has been markedly reduced, as compared with the results (circles) of the previous emitter pulsing arrangement. $Q_c(P)$ no longer falls monotonically towards zero as P is reduced below 25 bar. Rather, Q_c rises slightly at first, passes through a shallow maximum and then falls again. The reason for this behaviour is not properly understood but may perhaps be accounted for in the following terms. To start with, the emission current rises on reduction of pressure, because of enhanced charge multiplication processes close to the tips (Phillips & McClintock 1975); but this effect is eventually overwhelmed by the growing importance of vortex nucleation processes that, although greatly reduced by the tailored emitter pulses, have not been eliminated. However the main point, quite regardless of the precise physical mechanism, is that the procedure described has had the effect of doubling the range of pressures over which high-quality ion signals may be observed in practice and their corresponding velocities measured.

(*b*) *Velocity measurements*

As discussed above in §2*a*, it it essential to ensure that the drag on an ion resulting from excitation scattering is always negligible in comparison with that arising from roton creation. As an empirical check that this was indeed the case we have measured $\bar{v}$ as a function of T, while keeping all other parameters fixed, for a variety of physical conditions. A typical set of such data is shown in figure 20, with $E = 86$ V m^{-1} and $P = 25$ bar. They demonstrate convincingly that, although the effect of scattering clearly manifests itself in the slight decrease of $\bar{v}$ with increasing T above *ca.* 0.2 K, $\bar{v}$ has become reassuringly independent of T at 80 mK where most of the velocity measurements were made.

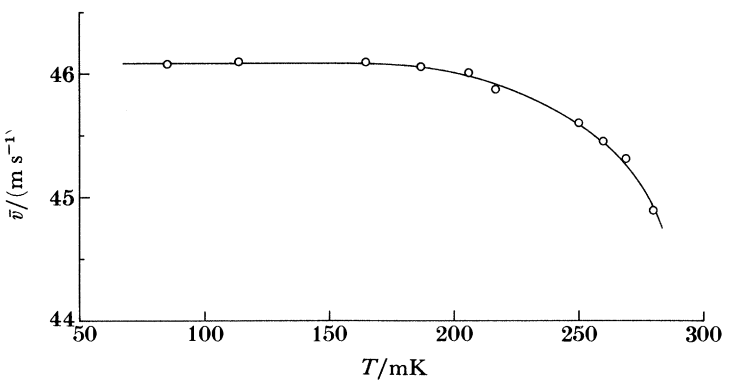

FIGURE 20. Temperature dependence of the ionic velocity. It is apparent that $\bar{v}$ becomes essentially independent of T below *ca.* 150 mK.

The velocity measurements that we have made fall naturally into two groups. First, forming by far the larger group, are the measurements for $E > 500$ V m^{-1}, which we have used for determination of the Landau critical velocity. Secondly, for $E < 500$ V m^{-1}, we shall see that the data depart significantly from (1.1); but not in the manner that would be expected on the basis of an onset of single-roton emission. We start by presenting the relatively high-field measurements.

Figure 21 plots the drift velocity $\bar{v}$ as a function of $E^{\frac{1}{3}}$(E is the electric field) as measured for

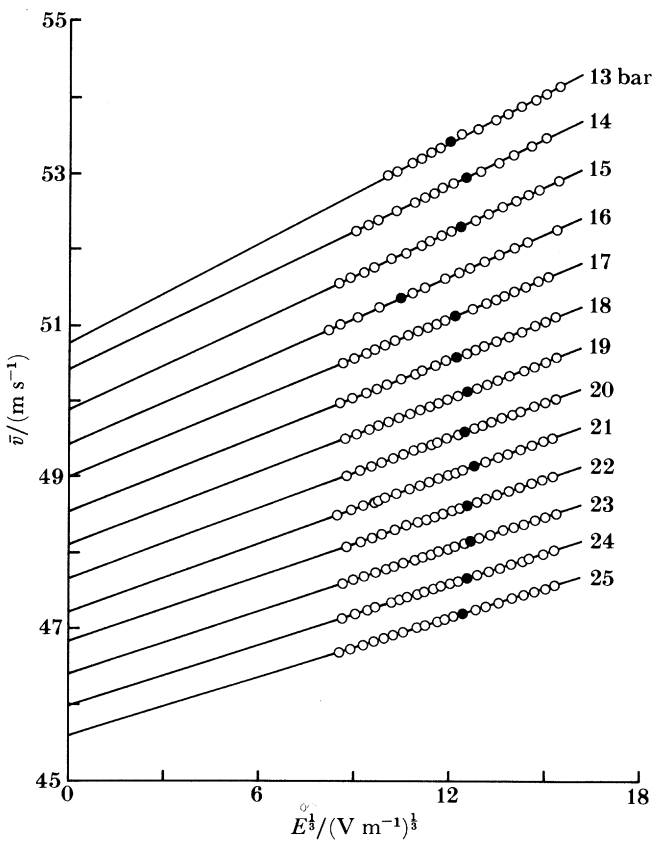

FIGURE 21. Measurements of $\bar{v}$ as a function of $E^{\frac{1}{3}}$ for several pressures in the range $13 \leqslant P \leqslant 25$ bar. The solid straight lines represent least-squares fits of (1.1) to the data, values of the fitting parameters being tabulated in the Appendix.

13 different pressures within the range 13 bar $\leqslant P \leqslant$ 25 bar. For each pressure, most of the measurements were made through use of the cross-correlation technique (§2*g*) that yields changes in $\bar{v}$ and they were scaled to absolute values by means of a single reference measurement (§2*f*) of $\bar{v}$, made at an intermediate value of E where the signal was relatively strong, indicated on the graph by the filled data point in each case. Some typical magnitudes of signals are plotted by the points of figure 5 and it is thus evident that there should have been no problems from space–charge spreading of the ion cloud. As the pressure was reduced towards 13 bar the signals became extremely weak, notwithstanding the use of the tailored-tip pulse technique described above. Bare-ion signals were, however, still detectable at pressures below 13 bar. With very careful optimization of all the operating parameters and prolonged signal averaging, the arrival of bare ions could be detected down to a minimum pressure of *ca.* $10\frac{1}{2}$ bar, but the signals were far too small to be of use in making the high-precision velocity measurements needed for the present research programme. For the range of electric fields above *ca.* 500 V m^{-1}, the data as plotted in figure 21 were linear in $E^{\frac{1}{3}}$ in accordance with (1.1).

For the lower electric fields, however, significant deviations from (1.1) were observed. A set of data spanning our full range of fields is plotted with an expanded ordinate scale for one pressure in figure 22. The points at low fields clearly curve downwards away from the behaviour predicted by (1.1). We discuss in more detail the possible origin of this unexpected behaviour

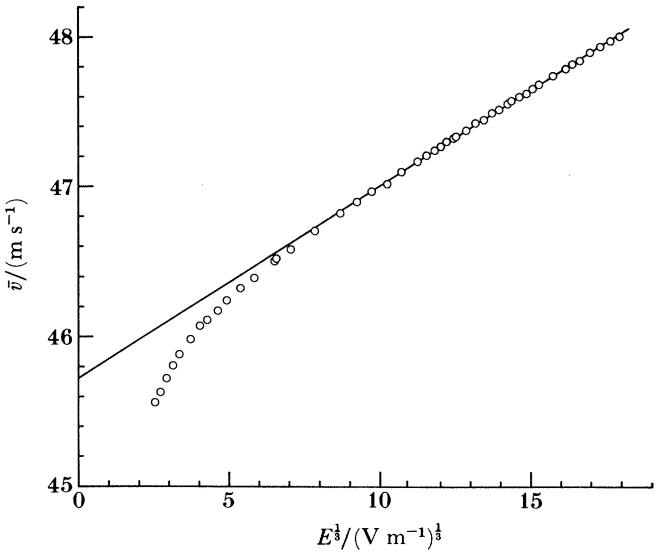

FIGURE 22. Measurements of $\bar{v}$ as a function of $E^{\frac{1}{3}}$ at a pressure of 25 bar, extending down to very low values of E. The solid straight line represents a fit of 1.1 to the data for $E > 500$ V m^{-1}.

in §4*c* but here we may note immediately, by inspection, that the 'droop' in the low-field data looks entirely different from any of the forms of $\bar{v}(E^{\frac{1}{3}})$ shown in figure 3 as the predicted effect of the onset of single-roton emission. In fact, it can be seen that $\bar{v}$ measured at the lowest value of E is actually smaller than the value of v_{L} defined by the intersection with the ordinate axis of a line fitted to the data for $E = 500$ V m^{-1}. Thus $(\bar{v}-v_{\mathrm{L}})/v_{\mathrm{L}}$ has apparently become negative, in sharp contradistinction to the behaviour that was anticipated in figure 3. Similar low-field characteristics to those of figure 3 have been found over a range of different pressures, but $\bar{v}$ measurements for $E < 500$ V m^{-1} become harder as P is reduced, owing to the reduction in the absolute magnitude of the signals.

All the measurements presented above were made with constant electric fields within the drift space. We have also investigated the effect of using the transient low-field technique described in §2*h*, on the assumption that it would permit the measurements to be extended to lower electric fields. The outcome was that, although this was indeed the case, it was not possible to extend the range to a useful extent. It was interesting to note, however, that the velocity measurements in question, although of somewhat inferior precision, were in excellent agreement with those obtained by the earlier techniques. Surprisingly, the signals still appeared to shrink at very low fields, even though the fields at the grids where the ions entered and left the drift space were relatively strong. A careful analysis of such signals showed, however, that the observed reduction in i_{c} at very low field apparently arose from a spreading of the ion disk. Within experimental error, the integrated area of the recorded signal was independent of the electric field. The effect was independent of the absolute magnitude of the signal and so may be presumed to be unrelated to space–charge effects (which should, in any case, have been negligible; see figure 5). It appears that the pulse broadening in question must be predominantly axial in character, because radial spreading would have resulted in a loss of ions to the side electrodes. The existence of the broadening has also been confirmed through direct measurement of the widths of signals at their half-heights. The percentage changes in width, $\Delta\tau_{\mathrm{w}}$, for the lower field data of figure 22 are plotted as a function of E in figure 23. Although there is

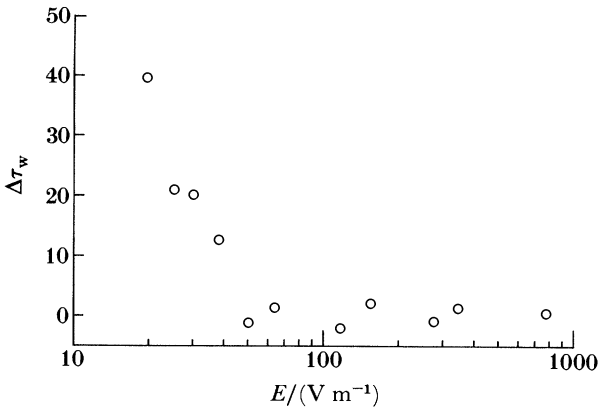

FIGURE 23. Measurements of the change in the width, $\Delta\tau_w$, of ion signals in weak electric fields, plotted as a function of the field, E.

considerable scatter (that could in principle be reduced by use of a curve-fitting procedure) it is clearly evident that the signal width increases rapidly with falling E at the lowest fields in the region of the droop.

Having established that data obtained by means of the transient low-electric-field technique were essentially identical to the more precise data obtained by the simpler techniques employed earlier, thus demonstrating that the shrinkage of i_c at low fields is in large measure associated with events occurring in the bulk of the liquid and not at the grids, we abandoned the technique. All of the velocity data presented in this paper were derived on the basis of the techniques discussed in §§2*f* and 2*g*.

(*c*) *Experimental errors*

The velocities were determined from the quotient of a length and a time, each of which was subject to a measure of experimental uncertainty.

The larger uncertainty lay, as in earlier parts of the research programme, in the length, L, of the drift space. As indicated above in §2*b*, L as determined from the measured separation of the grids G_3 and G_4 (figures 6 and 7) is known to $\pm 0.2\,\%$. There is also a small additional uncertainty in the effective value of L owing to the tendency of equipotentials to bulge through the holes of a grid when the electric fields differ on either side. The size of the resultant uncertainty will be of the order of the radius of a grid hole, or 0.05 mm in the present case. The net uncertainty in the cold value of L is therefore estimated at $\pm 0.3\,\%$. It represents a systematic error that will affect all velocity measurements equally.

There is also a systematic uncertainty in the determination of τ_{s1} for the absolute velocity measurements. This arises from the need (§2*f*) to make an explicit assumption about the form of the axial inhomogeneity of the charge disk. We assumed a linear dependence of charge density on position, which appears to be approximately correct but is certainly not exact. We can make an estimate of the size of the resultant error, however, by recomputing τ_{s1} from linear fittings of the data on both sides of the peak. This corresponds to the extreme (and obviously incorrect) assumption of a homogeneous ion cloud and an amplifier with a zero time constant, and it therefore represents something of a worst possible case. When this procedure is effected, we find values of τ_{s1} that are larger by about $0.25\,\%$. It seems reasonable, therefore, given the experimental observation that the ion density is much closer to being a linear variation with position than to being uniform, to guess that the net systematic uncertainty in τ_{s1} arising from

this cause is about $\pm 0.1\%$ at worst. The timebase of the Nicolet a.d.c., derived from a crystal-controlled clock, should not have been in error by more than a few parts per million at most, and is thus negligible by comparison.

Errors in the measurements of pressure appear to be negligible. Pressures were determined by means of a differentially pumped Texas Instruments gauge whose calibration was subsequently checked against a Budenberg dead-weight type absolute pressure gauge: the difference between the two instruments amounted to 0.07% at 25 bar. Systematic errors in the measured temperature of the helium (caused, for example, by the thermal boundary resistance between the sample and the lid of the chamber through which it was cooled) are considered unimportant in view of the relative temperature independence (figure 20) of the phenomena under study.

Random errors in the measured velocities arose from a variety of causes and varied greatly according to the physical conditions prevailing at the time. Their magnitude is best judged from the scatter of the data points about a smooth curve. The random uncertainty in velocity changes computed by means of the cross-correlation method (§2*g*) was usually negligible (seldom exceeding $\pm 0.05\%$) in comparison with that in the absolute velocity (§2*f*), which could reach $\pm 0.2\%$ or more, depending on the signal:noise ratio of the trace being analysed. Thus, the error in the intercept of a straight line fitted (see §4*a* below) to the data of figure 21 for any given pressure is effectively identical to the error in the determination of the absolute velocity for the relevant reference signal (filled point).

We conclude that the velocity measurements quoted are all subject to a systematic uncertainty of $\pm 0.4\%$ plus a variable random error that is usually smaller than this.

4. Discussion

(*a*) *Determination of the Landau critical velocity*

We have used the method of least squares to fit a straight line to the $\bar{v}(E^{\frac{1}{3}})$ data of figure 21 at each pressure. On the basis of (1.1) the intercept is then equal to the Landau critical velocity v_{L} and we may note immediately that v_{L} clearly increases with decreasing pressure as expected qualitatively, and in accordance with the predicted behaviour of figure 1. The experimental values of v_{L} obtained in this way are listed in the Appendix and are also plotted in figure 24 on an expanded scale to facilitate comparison with the theoretical prediction. The statistical errors involved in the least-squares fitting procedures, amounting typically to $\pm 10^{-4}$ m s^{-1} in the intercept, are found to be negligible in comparison to the systematic uncertainty of $\pm 0.4\%$ in its absolute value (§3*c*). We conclude therefore that, subject to the various caveats entered in §1*c*, our experimental values of v_{L} should be accurate to within $\pm 0.4\%$.

The solid curves of figure 24 are plots of (1.5) based on three different sets of published roton parameters; those of Donnelly (1972), of Maynard (1976) and of Brooks & Donnelly (1977); indicated respectively by the D, M and BD adjacent to the curves. It is immediately evident that the agreement of the Donnelly and the Brooks & Donnelly predictions with our data is remarkably good. The Donnelly curve is in almost perfect agreement with the data obtained near the solidification pressure, whereas the Brooks & Donnelly curve appears to be slightly better near 13 bar; in no case does the difference between the data and either of these two curves exceed 1.5%. The Maynard curve, on the other hand, appears to be significantly less satisfactory.

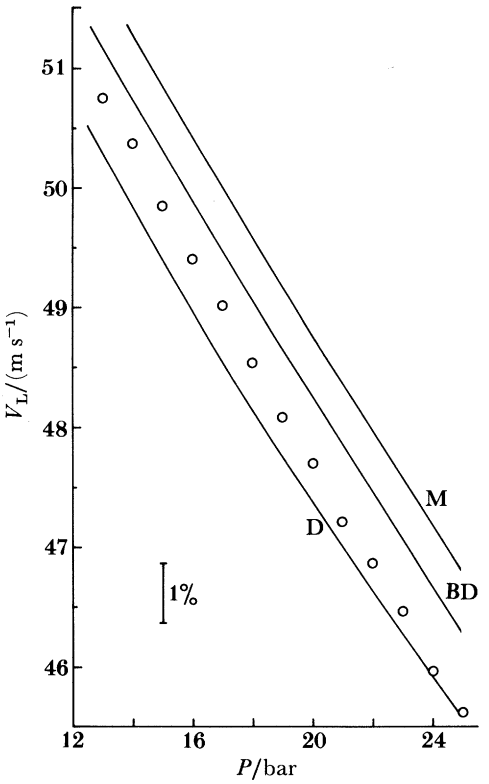

FIGURE 24. The Landau critical velocity for roton creation v_L as a function of pressure P. The circled points are experimental values obtained by fitting (1.1) to the data of figure 21 and the solid curves represent theoretical predictions (see text).

It is interesting to note that our experimental values of $v_L(P)$ show a stronger pressure dependence than expected on the basis of any of the sets of roton parameters; a conclusion which would, of course, still be valid even if we had somehow mis-estimated the systematic error in our measurements. If, for example, our cell were about 1 % longer than we believe to be the case, all our data points in figure 24 should then be scaled up by the same factor, which would clearly lead to excellent agreement with the Brooks & Donnelly curve at 17 bar, but to significant discrepancies at 13 and 25 bar.

We have investigated the effect of attempting to make explicit allowance for the droop in $\bar{v}(E^{\frac{1}{3}})$ seen at lower fields (figure 22) than those of figure 21, because it could reasonably be argued that the incipient droop could perhaps give rise to an additional source of systematic error. In doing so, we re-fitted the data on the assumption that (1.1) should be replaced by an equation of the form

$$\bar{v} = v_L + AE^{\frac{1}{3}} + CE^{-1}, \tag{4.1}$$

which gives quite a good (empirical) fit to the data of figure 21, where C is an additional constant. The net effect was to increase the scatter in the fitted values of v_L but without moving them significantly either up or down. The values of C turned out to be both positive and negative. We decided, therefore, that all of the data in figure 21 should be regarded as being within the linear regions of their respective $\bar{v}(E^{\frac{1}{3}})$ characteristics and that no advantage was to be gained from fitting them to (4.1) rather than to (1.1).

We may conclude that the quality of the agreement between the predicted and experimental values of $v_L(P)$ should in fact be regarded as highly gratifying. The small discrepancies that

are observed are almost certainly not from any unforseen deficiency of the Landau excitation model but, rather, from the relatively large uncertainty in the values of the roton parameters under pressure. Donnelly & Roberts (1977) have remarked that reliable inelastic neutron scattering data are lacking in this region of the helium phase diagram and that some accurate values, based on the improved neutron scattering techniques now available, are much to be desired. The present results would certainly appear to lend further support to this point of view because they have clearly demonstrated that the pressure dependence of $\Delta/\hbar k_0$ is stronger than was hitherto believed to be the case.

(*b*) *The matrix element for roton-pair emission*

It is immediately evident from inspection of figure 21 that the straight lines on which the data fall are becoming considerably steeper as the pressure is reduced. This implies that the strength of the roton-pair emission process is decreasing or, equivalently, that the modulus of the relevant matrix element (see I) becomes smaller with decreasing pressure. Such a conclusion is consistent with the results reported for a very much more restricted range of pressures in III. In fact, the gradients, A, of the fitted lines are found to decrease by some 70% between 25 and 13 bar; they are tabulated in the Appendix. It is straightforward to extract values of the square of the matrix element by use of equations (4.4) and (5.7) of I which, when a numerical factor derived by Bowley & Sheard (1977) is also included, become

$$\beta = k_0^4 |V_{k_0,k_0}|^2 \mu/(2\pi^2\hbar^3 v^2) \tag{4.2}$$

and

$$(v - v_L)^3 = 0.893\,(3eE/\beta m_i) \tag{4.3}$$

respectively; whence the modulus of the matrix element

$$|V_{k_0,k_0}| = (52.88\hbar^3 v^2 e/k_0^4 \mu m_i A^3). \tag{4.4}$$

In evaluating $|V_{k_0,k_0}|$ by use of (4.4) and our experimental measurement of A, we have used the Brooks & Donnelly (1977) roton parameters together with our own measured values (Ellis

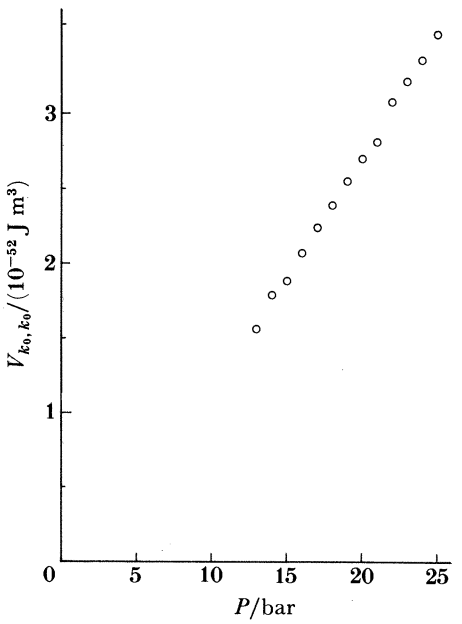

FIGURE 25. Experimental values of the matrix element for roton-pair creation $|V_{k_0,k_0}|$ derived from the data of figure 21 by use of (1.1) and (4.4) and plotted as a function of pressure, P.

et al. 1983) of the ionic effective mass m_i. Values of $|V_{k_0,k_0}|$ deduced in this way are plotted as a function of pressure in figure 25.

The pressure dependence of the matrix element is rather stronger than was implied by the results of III. Indeed, it is falling so rapidly with decreasing pressure that a linear extrapolation would imply a complete cessation of roton-pair emission below *ca.* 3 bar. The most significant consequence of decreasing the pressure is probably the increase in the radius of the ion (Springett & Donnelly 1966), so that one possible interpretation of figure 25 is that the unknown mechanism by which pairs of rotons are created is entirely suppressed if the ion becomes too large. An alternative explanation, equally consistent with the data, is that V_{k_0,k_0} passes through zero, changing sign at *ca.* 3 bar; perhaps because of some type of interference process occurring between the emitted rotons. If this were the case, V_{k_0,k_0} would be expected to start increasing again at lower pressures. Of course, there is no physical basis for a linear extrapolation *per se* in figure 25 and a shallow curve intersecting the abscissa axis close to the origin would look equally plausible. Further progress will require the development of an explicit physical model of the creation mechanism.

It is unfortunate that the crossing of $v_L(P)$ with the critical velocity $v_c(P)$ for vortex creation (figure 1) effectively precludes any attempt to follow the roton-pair emission matrix element experimentally down to lower pressures. If, for some reason, pair emission does not occur at low pressures, it remains possible that roton emission in larger groups or, indeed, singly could take over as the dominant dissipative mechanism and could, in principle, be identified from the electric-field dependence of $\bar{v}$. It seems unlikely, however, that it will ever be possible to investigate this intriguing question in the case of the normal negative ion. The dissipative behaviour of the fast negative ion, however, remains an entirely open question. It is clear (Eden & McClintock 1983) that it creates rotons rather than vortex rings under the saturated vapour pressure, but the measurements in question were of insufficient precision and at too high a temperature to establish whether or not the rotons were being created in pairs. The clarification of this particular point will provide an interesting topic for future studies.

(*c*) *Ion motion in very weak electric fields*

We have already remarked in §3*b* that the deviations of the measured $\bar{v}(E^{\frac{1}{3}})$ from (1.1) below *ca.* 500 V m^{-1} (figure 22) are entirely different in form to what would be expected (figure 3) if single-roton emission were important in this range of electric fields. Neither does the low-field droop in $\bar{v}(E^{\frac{1}{3}})$ appear to be associated with momentum loss due to the scattering of thermal excitations, as could be the case if the sample of helium in the cell were insufficiently cold. The results shown in figure 20, recorded at an electric field where significant deviations from (1.1) are readily apparent, clearly demonstrate that $\bar{v}$ and hence the magnitude of the droop, are independent of temperature within experimental error at least up to 150 m K. Although the existence of these deviations does not appear to have affected our measurements of $\bar{v}_L$, based on data recorded at higher electric fields, it is of interest to speculate on their possible origin; it may also, perhaps, be of relevance to future experiments on He II in the millikelvin range.

It should be noted that precise measurements of $\bar{v}$ in the region of the droop are not easy because of the weakness of the signals (figure 5) in very low electric fields and also because of the need to measure what are, in fact, very small deviations (*ca.* 1% at most) from (1.1). It was only when the cross-correlation technique of §2*b* had been fully developed and brought into use that reproducible data such as those of figure 22 could be recorded. The lowest value

of E at which measurements could be made was determined, in practice, by the attenuation of the signal.

We have found that the existence of the droop is insensitive to changes in pressure or temperature or the absolute magnitude of the signal. Reduction of i_c by a factor of two is easily effected by a small adjustment to the negative-going peak in the tip pulse, but it has no discernible effect on the magnitude of the droop. The only parameter we have found that does significantly affect the droop is the size of the positive bias on the emission tips while they are resting in between emission events (figure 10*a*). Here, the effect is quite definite and reproducible. In figure 26, we plot measured values of $\bar{v}(E^{\frac{1}{3}})$ at low fields on considerably expanded scales, first running in our normal mode with positive bias applied (triangles); second, without the positive bias (circles). While these results were being recorded, all other physical parameters were held constant and the only difference between them, therefore, is the presence or absence of the bias. It seems clear that, while the bias has no significant effect on $\bar{v}$ for $E > 500$ V m^{-1}, it exerts an important influence on whatever physical mechanism is responsible for the droop at lower fields.

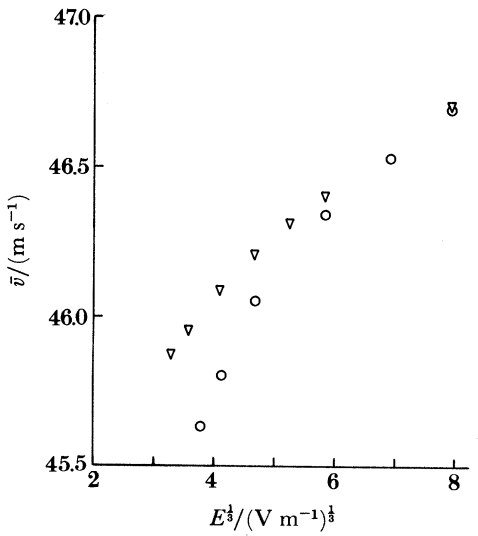

FIGURE 26. The ionic drift velocity $\bar{v}$ as a function of $E^{\frac{1}{3}}$, measured in very weak fields for two different ion injection modes (see text).

The reason that the tailored-tip pulse with positive bias was introduced in the first place was, as discussed in §3*a*, to reduce the amount of vorticity believed to be entering the drift space. If we accept that this picture is correct, then it is natural to conclude that the droop is likely to be caused by an interaction between the ions and vortex lines or rings that they encounter during their flight between G_3 and G_4.

Unfortunately it is difficult to place these ideas on a more quantitative basis at the moment. There is no doubt, in the light of III, that the operation of the emission tips must result in the creation of some vorticity, and it is to be expected that this will tend to diffuse throughout the cell. The positive bias on the tips will help to hold back any charged vorticity, preventing it from entering the drift space; but it is to be anticipated that, if reconnection processes (Schwarz 1982) occur, elements of vortex line will be created that are not charged and that will therefore be unaffected by the bias. It is to be expected that, with the tips regularly pulsing,

the average density of vorticity will increase towards some equilibrium value where vortex annihilation processes exactly balance the production rate. It is by no means clear, however, what these annihilation mechanisms might be. The decay mechanism of turbulence at temperatures above 1 K is now quite well understood (Schwarz 1978, 1982) and depends on the presence of normal fluid damping. Such damping will, of course, be virtually non-existent at the temperatures of the present experiments and so the mechanism in question must be presumed inoperative. Given the continual (through periodic) injection of vorticity from our field emitters, and given that the density of vorticity does not in practice appear to increase towards infinity (which would presumably preclude observation of any bare ion signal at all), it is clear that some other line-destruction mechanism must come into operation at low temperatures.

In the present state of understanding, therefore, it is difficult to make any further progress in attempting to account for the droop. To do so, we will require a physical model for vortex annihilation in the absence of damping and, in addition, a model for the ion–vortex interaction in the absence of damping. What we can conclude, however, is that it appears extremely likely on the basis of the evidence of figures 19, 22, 23 and 26 that the motion of ions in our cell under the influence of very weak fields is markedly affected by the presence of vorticity.

There are three further points that should be made in this context. First, the fact of there being charged vorticity present in the cell immediately introduces the possibility of an induced motion of the superfluid; the force exerted by the electric field on the charged vorticity will not be exactly uniform over the cross section of the cell and it might, therefore, be expected to result in some sort of convective motion of the aether in which v_L is being measured. One could, for example, envisage an axial flow of superfluid towards the collector, with the return stream passing down the outside of the electrode structure (figure 6). Although the forces involved in producing such a motion would certainly be extremely weak, they might eventually produce a significant effect, given that the fluid is inviscid. All we can say in response to such a suggestion is that the measured velocities above 500 V m^{-1} are very accurately reproducible and do not change with time. Neither do they vary with, for example, the signal repetition rate or with the absolute magnitude of the tip pulse; both of which would be expected to have an effect on the average force, if any, exerted by the electric fields on the superfluid. Thus, although the effect is very hard to estimate quantitatively, the empirical evidence all points towards the conclusion that its magnitude is negligible.

The second point is that a droop in $\bar{v}(E^{\frac{1}{3}})$ may conceivably be intrinsic to ion motion in HeII under weak electric fields at very low temperatures, independent of the method of ion injection. Awschalom & Schwarz (1984) have shown that, as had long been suspected (Vinen 1963), HeII is apparently always threaded by an array of metastable vortex lines, regardless of its previous history. Although their experiments refer to the viscous normal-fluid régime above 1 K, it seems highly likely that equivalent behaviour will also occur in the millikelvin range. The extent to which ion motion will be affected depends, of course, on the density of the remanent vorticity at these temperatures and, at the time of writing, has been neither measured nor calculated.

Finally, it should be noted that one cannot plausibly account for the discrepancy between the predicted and measured pressure dependences of v_L (figure 24) in terms of the droop. If the droop is indeed associated with the presence of vorticity in the drift space, then one would expect its magnitude to become larger with decreasing pressure in view of the increased rate (see III) of vortex nucleation. (Experimental measurements are difficult because of the severe

attenuation of the signal at low pressures and electric fields, but they are not inconsistent with this supposition.) If the incipient droop were distorting the fits of (1.1) to the data of figure 21, the net effect would be to increase the gradient in each case and to pull the ordinate intercept (and thus v_L) downwards. Consequently, the result of the droop would, if anything, be to cause the measurement of anomalously low values of v_L, the effect becoming less pronounced at the higher pressures. This would tend to weaken the apparent pressure dependence of v_L, thereby giving rise to a discrepancy in the opposite direction to that observed.

5. Conclusion

The principal conclusions to be drawn from the experiments may be summarized as follows.

1. The Landau critical velocity for roton creation in HeII has been measured precisely for the first time, with results as illustrated in figure 24 and tabulated in the Appendix.

2. The experimental values of v_L agree to within better than 1.5% with those predicted by Landau's excitation model of HeII, as calculated from (1.5) on the basis of the Brooks & Donnelly (1977) tabulation of roton parameters.

3. There are, however, significant deviations between the measured and calculated values of v_L, lying outside our estimated experimental error and becoming larger at the higher pressures. These should probably be regarded as an indication that the pressure dependence of $\Delta/\hbar k_0$ is slightly stronger than previously thought and hence that the Brooks & Donnelly roton parameters become progressively less accurate with increasing pressure. The best way to resolve the discrepancies would be through the application of modern inelastic neutron scattering techniques to the relevant part of the ^{4}He phase diagram.

4. The magnitude of the roton-pair emission matrix element falls rapidly with decreasing pressure. A linear extrapolation of the data acquired for $P \geqslant 13$ bar down to lower pressures implies that the pair-emission process is extinguished completely at a pressure of *ca.* 3 bar.

5. No evidence has been found to support the suggestion that single-roton emission processes might become an important source of dissipation in very weak electric fields.

6. The deviations in the form of $\bar{v}(E^{\frac{1}{3}})$ from (1.1) are probably attributable to a form of ion-vortex scattering but further work, both theoretical and experimental, will be needed to elucidate the physical processes that are involved.

It is a pleasure to acknowledge valuable discussions with many colleagues and acquaintances including, especially, A. M. Guénault, N. W. Kerley, G. R. Pickett, K. W. Schwarz and W. F. Vinen who was kind enough to read and comment in detail upon the initial version of the typescript. To R. M. Bowley we owe a particular debt of thanks for his generous help and imaginative insights, and for his continuing encouragement of this work over many years. The experiments were heavily dependent on the skilful technical assistance of D. H. Bidle, G. Caley and I. E. Miller. The research was supported by the Science and Engineering Research Council to whom one of us (T.E.) is also indebted for the provision of a research associateship.

References

Allum, D. R., McClintock, P. V. E., Phillips, A. & Bowley, R. M. 1977 *Phil. Trans. R. Soc. Lond.* A **284**, 179–224 (referred to in text as I).

Andrei, E. Y. & Glaberson, W. I. 1980 *Physics Lett.* A **79**, 431–434.

Awschalom, D. D. & Schwarz, K. W. 1984 *Phys. Rev. Lett.* **52**, 49–52.

Bowley, R. M. 1984 *J. Phys.* C **17**, 595–613.
Bowley, R. M. & Sheard, F. W. 1977 *Phys. Rev.* B **16**, 244–254.
Bowley, R. M., McClintock, P. V. E., Moss, F. E., Nancolas, G. G. & Stamp, P. C. E. 1982 *Phil. Trans. R. Soc. Lond.* A **307**, 201–260 (referred to in text as III).
Brooks, J. S. & Donnelly, R. J. 1977 *J. Phys. Chem. Ref. Data* **6**, 51–104.
Donnelly, R. J. 1972 *Physics Lett.* A **39**, 221–222.
Donnelly, R. J. & Roberts, P. H. 1977 *J. Phys.* C **10**, L683–685.
Eden, V. L. & McClintock, P. V. E. 1983 In *75th Jubilee Conference on Helium-4* (ed. J. G. M. Armitage), pp. 194–195. Singapore: World Scientific.
Ellis, T., McClintock, P. V. E., Bowley, R. M. & Allum, D. R. 1980*a* *Phil. Trans. R. Soc. Lond.* A **296**, 581–595 (referred to in text as II).
Ellis, T., Jewell, C. I. & McClintock, P. V. E. 1980*b* *Physics Lett.* A **78**, 358–360.
Ellis, T., McClintock, P. V. E. & Bowley, R. M. 1983 *J. Phys.* C **16**, L485–489.
Iordanskii, S. V. 1968 *Zh. éksp. teor. Fiz.* **54**, 1479–1493; translated in *Soviet Phys. JETP* **27**, 793–800 (1968).
Maynard, J. 1976 *Phys. Rev.* B **14**, 3868–3891.
Muirhead, C. M., Vinen, W. F. & Donnelly, R. J. 1984 *Phil. Trans. R. Soc. Lond.* A **311**, 433–467.
Nancolas, G. G., Bowley, R. M. & McClintock, P. V. E. 1985 *Phil. Trans. R. Soc. Lond.* A **313**, 357–606 (referred to in text as IV).
Ostermeier, R. M. 1973 *Phys. Rev.* A **8**, 514–529.
Phillips, A. & McClintock, P. V. E. 1973 *Physics Lett.* A **46**, 109–110.
Phillips, A. & McClintock, P. V. E. 1975 *Phil. Trans. R. Soc. Lond.* A **278**, 271–310.
Rayfield, G. W. 1966 *Phys. Rev. Lett.* **16**, 934–936.
Schwarz, K. W. 1972 *Phys. Rev.* A **6**, 837–844.
Schwarz, K. W. 1978 *Phys. Rev.* B **18**, 245–262.
Schwarz, K. W. 1982 *Phys. Rev. Lett.* **49**, 283–285.
Sheard, F. W. & Bowley, R. M. 1978 *Phys. Rev.* B **17**, 201–203.
Springett, B. E. & Donnelly, R. J. 1966 *Phys. Rev. Lett.* **17**, 364–367.
Vinen, W. F. 1963 In *Liquid helium: Proceedings of the International School of Physics 'Enrico Fermi', Course XXI* (ed. G. Careri), p. 336. New York: Academic Press.

Appendix: Tabulation of principal experimental results

We present in table 1 a synopsis of the principal experimental results reported in this paper. For each of several pressures, we list the gradient and intercept found by fitting (1.1) to the data of figure 21 by the method of least squares. The intercept gives the Landau critical velocity v_L directly; the modulus of the matrix element for pair emission has been calculated from the gradient in each case through use of (4.4), as described in §4*b*, and is also listed. The measurements of v_L are subject to a systematic uncertainty of $\pm 0.4\,\%$ that affects all of them equally, plus a variable random error that is smaller than this. The maximum experimental error in the matrix element is believed to be of the order of a small percentage.

Table 1. Principal experimental results

P/bar	$v_L/(\mathrm{m\ s^{-1}})$	$A/(V^{\frac{1}{3}}\,\mathrm{m^{\frac{2}{3}}\,s^{-1}})$	$\lvert V_{k_0,k_0}\rvert/(10^{-52}\,\mathrm{J\ m^3})$
13	50.75	0.218	1.56
14	50.37	0.200	1.79
15	49.83	0.194	1.88
16	49.40	0.183	2.07
17	49.02	0.174	2.24
18	48.53	0.167	2.39
19	48.08	0.160	2.55
20	47.70	0.155	2.70
21	47.22	0.150	2.81
22	46.87	0.142	3.08
23	46.47	0.138	3.22
24	45.97	0.133	3.36
25	45.62	0.129	3.54